Jang *et al. Microstructures* 2024;4:2024016
DOI: 10.20517/microstructures.2023.67

Microstructures

Review

Open Access

Check for updates

Reduced dimensional ferroelectric domains and their characterization techniques

Jinhyuk Jang[1], **Si-Young Choi**[1,2,3]

[1]Department of Materials Science and Engineering, Pohang University of Science and Technology, Pohang 37673, Republic of Korea.
[2]Department of Semiconductor Engineering, Pohang University of Science and Technology, Pohang 37673, Republic of Korea.
[3]Center for Van der Waals Quantum Solids, Institution of Basic Science, Pohang 37673, Republic of Korea.

Correspondence to: Prof. Si-Young Choi, Department of Materials Science and Engineering, Pohang University of Science and Technology, 77 Cheongam-Ro, Pohang 37673, Republic of Korea. E-mail: youngchoi@postech.ac.kr

How to cite this article: Jang J, Choi SY. Reduced dimensional ferroelectric domains and their characterization techniques. *Microstructures* 2024;4:2024016. https://dx.doi.org/10.20517/microstructures.2023.67

Received: 1 Nov 2023 **First Decision:** 5 Dec 2023 **Revised:** 27 Dec 2023 **Accepted:** 23 Jan 2024 **Published:** 29 Mar 2024

Academic Editor: Nazanin Bassiri-Gharb **Copy Editor:** Fangling Lan **Production Editor:** Fangling Lan

Abstract

Ferroelectricity is one of the most major physical phenomena in electronic devices due to its sustainable polarity in the absence of an external electric field and its switchability in response to external stimuli. In alignment with the industry trend towards increasingly integrated devices, research into smaller-sized ferroelectric materials becomes indispensable. In the pursuit of achieving the pinnacle of device miniaturization, recent studies have unveiled materials exhibiting sub-nanometric, unit cell-level domains. Concurrently, advances in transmission electron microscopy-based structural characterization techniques have been made, enabling in-depth analysis of the intricate properties of these miniaturized ferroelectric materials. This review highlights the structural mechanism of ferroelectricity in a reduced scale, as well as the recent advancements in electron microscopy techniques for characterizing miniaturized ferroelectric domains, particularly in the fields of *in-situ* biasing and atomic scale imaging. We believe that this work will provide structural insights for engineering and characterizing ferroelectrics for the design of downsized high-density memory devices at the quantum limit.

Keywords: Ferroelectrics, domains, thin films, miniaturization, atomic structure, transmission electron microscopy

INTRODUCTION

Ferroelectricity is one of the most major physical phenomena that is applicable to electronic devices because

of its sustainable polarity without an external electric field and its switchability by external stimuli[1] [Figure 1A]. These properties of ferroelectric materials make them highly suitable for applications in non-volatile memories, information storage devices such as FeRAM (Ferroelectric Random Access Memory) and FeFET (Ferroelectric Field Effect Transistor). To apply ferroelectric materials in devices effectively, it is crucial to understand the structure and properties of the polarization they exhibit. This involves investigating the polarization mechanisms, which explain how polarization occurs, and the switching dynamics that control polarization. Depending on the desired form of the component, the properties of ferroelectric materials should be tuned and designed accordingly. Particularly, with the trend toward miniaturization in the device industry, the downsizing of ferroelectric materials has become increasingly important. Simultaneously, various techniques, such as transmission electron microscopy[2] (TEM), for analyzing the structure and characteristics of miniaturized ferroelectric materials are being developed and integrated to meet these demands [Figure 1B]. For example, high-angle annular dark-field scanning TEM (HAADF-STEM) can directly show the breaking of inversion symmetry and polarization in materials at the atomic scale, as illustrated in Figure 1C.

In this paper, we aim to provide a brief overview and classification of oxide-based ferroelectrics, particularly focusing on their unique characteristics and the various mechanisms underpinning their extensive research. We will discuss why oxide-based ferroelectrics have been predominantly studied and what potential benefits can be expected from them. Subsequently, we will delve into various research endeavors related to the scaling of ferroelectrics, primarily considering aspects related to thickness and width. Lastly, we review techniques for analyzing the properties of ferroelectrics and explore their applications in research.

FERROELECTRIC MATERIALS

The pioneering research into ferroelectric phenomena began with the hysteresis measurements of Rochelle Salt in 1921[3]. Subsequently, in 1941, ferroelectricity was discovered in the oxide perovskite material called $BaTiO_3$, which sparked expectations that ferroelectricity could manifest in simple structures. This led to the active exploration and discovery of new ferroelectric materials in perovskite oxides such as $Pb(Zr,Ti)O_3$[4] and $LiNbO_3$[5]. A brief history of representative oxide-based ferroelectrics is summarized in Table 1. Alongside the discovery of these materials, research on non-volatile memory based on ferroelectrics began in the 1950s[6], capitalizing on the characteristic of ferroelectric polarization states representing binary states. FeRAM and FeFET[7], two significant developments in this field, were proposed in 1952 and 1963, respectively, garnering considerable attention in the academic community. However, they faced limitations, such as endurance, retention, scalability (with device thickness typically above 100 nm), and compatibility issues in thin-film performance.

As a result, there have been research efforts to synthesize ferroelectric materials as thin films with the aim of creating small electronic devices. Around the same time, there were significant efforts to create thin films of superconductors such as $YBa_2Cu_3O_7$, leading to advancements in the technology to epitaxially deposit them in a single crystal form[8,9]. This progress allowed for the control of ferroelectricity coupled with lattice structures through epitaxial control. The development of thin films of layered ferroelectrics, such as $SrBi_2Ta_2O_9$, aimed to address endurance issues[10]. Research has also been conducted on very thin ferroelectric films such as $PbTiO_3$[11] and $BiFeO_3$[12]. Additionally, as the thickness of thin films has gradually reduced, studies related to the manifestation of ferroelectric properties in non-ferroelectric materials, such as $SrTiO_3$, have begun to emerge[13].

In recent years, a significant breakthrough occurred in the field of ferroelectric research with the discovery that HfO_2, which had been widely used as a high-k (permittivity) gate insulator in the semiconductor

Table 1. A brief summary of representative materials in oxide-based ferroelectrics

Ferroelectrics	$BaTiO_3$	$Pb(Zr,Ti)O_3$	$LiNbO_3$	$SrBi_2Ta_2O_9$	$BiFeO_3$ thin film	HfO_2
Discovered year	1941	1949	1949	1960	2003	2011
Structure	Perovskite	Perovskite	Perovskite	Aurivillius	Perovskite	Fluorite
Ferroelectric mechanism	Displacive Order-disorder	Displacive Lone pair	Order-disorder	Improper	Lone pair	Improper
Remnant polarization ($\mu C/cm^2$)	25	20-100	10-30	30-70	50-100	1-50

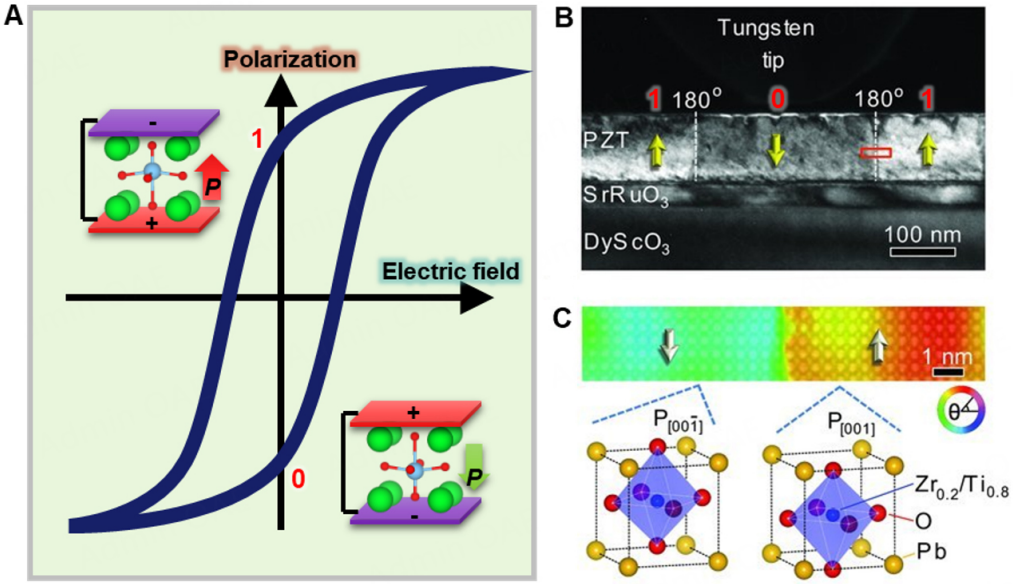

Figure 1. Ferroelectric characteristic and its domain structure. (A) A schematic of a typical ferroelectric P-E hysteresis loop. Based on the polarization direction, two distinct binary digits can be differentiated. (B) Dark-field TEM image showing ferroelectric domains with 180° domain walls in $Pb(Zr,Ti)O_3$ thin film. (C) HAADF-STEM image overlaid with its polarization angle map and corresponding $Pb(Zr,Ti)O_3$ structure. Color wheel means the orientation of the polarization at each unit cell. Reproduced with permission[3]. Copyright 2012, WILEY-VCH Verlag Gmbh & Co. KGaA, Weinheim.

industry, exhibited robust ferroelectric properties when doped with silicon[14]. This discovery, made in 2011, led to an explosion of research related to inducing ferroelectricity in HfO_2 through doping with elements such as Zr and Y[15-17]. The introduction of this new paradigm in ferroelectric research, driven by the discovery of new materials, has sparked a multitude of studies aimed at realizing ferroelectricity at even smaller thicknesses and applying it to highly dense memory devices.

Two-dimensional (2D) ferroelectric materials, being inherently thin, offer significant advantages in terms of scaling. Active research is being conducted on quasi-2D materials using oxide membranes such as $BiFeO_3$[18] and $CsBiNb_2O_7$[19]. The most well-known 2D materials include transition metal dichalcogenides such as MoS_2[20], with numerous reports of ferroelectricity in materials such as SnTe[21], In_2Se_3[22], and $CuInP_2S_6$[23,24]. These 2D materials possess stable surfaces free of dangling bonds and are less affected by substrates, which is advantageous. Most 2D ferroelectrics exhibit Curie temperatures above room temperature and have varied electronic bandgaps, making them suitable for practical applications[25]. A prime example is SnTe, which can exhibit in-plane ferroelectricity down to a one-unit-cell limit at low temperatures[21]. In addition, $CuInP_2S_6$, a room-temperature ferroelectric with a layered structure, exhibits out-of-plane ferroelectric polarization due to the off-centering of Cu and In ions from the center of sulfur octahedra, with polarization observed even in layers as thin as 4 nm[23].

As materials have become miniaturized, there has been a growing need for a better understanding of ferroelectricity within these materials. Consequently, research into techniques for characterizing such ferroelectricity has seen significant advancements. The ferroelectric properties in thin films often exhibit notable differences from those in bulk materials, which has spurred further investigations.

FERROELECTRIC MECHANISM

The foundation for the development of new ferroelectric materials begins with a structural understanding of the underlying mechanisms responsible for ferroelectricity. Ferroelectricity typically arises from the breaking of inversion symmetry in ionic crystal structures[26]. It can be explained through various mechanisms, including proper ferroelectricity, often associated with displacive mechanisms, order-disorder mechanisms, and anisotropic lone-pair effects. For instance, the tetragonal phase of $BaTiO_3$ occurs at temperatures below the Curie temperature of 120 °C[27]. In this material, the tetragonal lattice structure is established with Ba ions as the reference points, and displacements of Ti^{4+} ions and oxygen octahedra give rise to ferroelectricity[28] [Figure 1]. Almost concurrently, an order-disorder type ferroelectric model was proposed for $BaTiO_3$, which, in reality, exhibits mixed characteristics[29-31]. According to the order-disorder model for $BaTiO_3$, the disorder in the paraelectric phase is related to the positioning of Ti ions. This characteristic of $BaTiO_3$ is well-illustrated through Raman spectroscopy, where the high-temperature Raman spectra show two broadbands at 260 and 530 cm^{-1}, indicating the disorder of Ti ions[32,33]. In general, the order-disorder mechanism involves electric dipoles aligning in one direction as the temperature drops below the Curie point (T_C), thereby acquiring ferroelectric properties. This mechanism is well-known in materials such as KH_2PO_4[34] and $NaNO_2$[35].

Another example, $BiFeO_3$, exhibits ferroelectricity due to the presence of Bi^{3+} with $6s^2$ lone pairs[36]. $Pb(Zr,Ti)O_3$ encompasses characteristics of both cases mentioned above, and it has a large remnant polarization of about 82 $\mu C/cm^2$[37]. It exhibits ferroelectricity through the relative displacements of oxygen octahedra and Ti^{4+}/Zr^{4+} ions, in addition to the presence of $6s^2$ lone pairs from Pb^{2+}[38]. In the case of typical displacive ferroelectricity, materials often face competition between polar distortion and BO_6 octahedral rotation, influenced by the Goldschmidt tolerance factor. As a result, among the numerous perovskite materials, those with ferroelectric properties remained relatively undiscovered or less well-known[39].

On the other hand, improper ferroelectricity has been discovered in recent years and found to result from polarization-coupled geometric distortion of polyhedral[40,41] or magnetic ordering[42] as in hexagonal-$YMnO_3$, layered perovskite such as $Ca_3Ti_2O_7$, and orthorhombic-$TbMnO_3$ materials. Strong hybridization between the transition metal and oxygen ions is not necessary in improper ferroelectricity, so non-d^0 transition metal can be introduced, allowing magnetoelectric coupling[43]. Boracite is an example of improper ferroelectric and has attracted interest due to its multiferroic properties[44,45]. It has a complex structure denoted as $M_3B_7O_{13}X$ (where M is a divalent metal and X is a halogen). Using $Mg_3B_7O_{13}Cl$ as an example, the material transitions from a cubic phase at high temperatures to an orthorhombic phase through structural shearing as the temperature decreases, leading to a ferroelectric transition[46,47]. The spontaneous polarization is about 1 $\mu C/cm^2$. Boracite can have six different domain states, each separated by straight boundaries. It can simultaneously possess charge-neutral 180° and charged 90° domain walls, making it a promising material for electronic applications[48,49].

More specifically, within the category of improper ferroelectrics, there exists a type known as hybrid improper ferroelectrics[41]. In this case, polarization arises from a complex distortion pattern that involves more than two nonpolar lattice modes with different symmetries. An example of a hybrid improper ferroelectric is the layered perovskite $Ca_3Mn_2O_7$, in which polarization is manifested through a combination

of octahedral rotation mode and tilt mode. In addition, the reversal of polarization can be achieved by distortion in just one of these modes, either rotation or tilt. In the case of interfacial engineered materials, such as ferroelectric $PbTiO_3$ and paraelectric $SrTiO_3$ superlattices, improper ferroelectricity can emerge due to a unique type of atomic rearrangement[50]. First-principle calculations indicate that the ground state is not purely ferroelectric; rather, it predominantly involves the antiferrodistortive rotation of oxygen atoms. Polarization can arise from the coupling of two in-phase and out-of-phase octahedral rotational modes. Notably, these materials exhibit a very large dielectric constant that remains unaffected by temperature changes.

As illustrated in Figure 2, hexagonal $YMnO_3$, unlike the typical perovskite structure, has a B-site Mn with a two-dimensionally networked MnO_5 polyhedra structure[51]. These MnO_5 triangular bipyramids can geometrically buckle to induce inversion symmetry breaking. Similarly, layered perovskites have BO_6 octahedra that are two-dimensionally networked such as $YMnO_3$, aligned in-plane[52]. The way these octahedra rotate determines the ferroelectric polarization, and the polarization expressed as layer-resolved polarization is present in-plane. Structures such as Ruddlesden-Popper $A_{n+1}B_nO_{3n+1}$, Aurivillius $Bi_2O_2(A_{n-1}B_nO_{3n+1})$, and Dion-Jacobson $A'(A_{n-1}B_nO_{3n+1})$ belong to the layered perovskite structure[53] [Figure 2B].

In this way, oxygen octahedra and perovskite structures can also play a role in inducing ferroelectricity. The control of perovskite structures is achieved in thin films through factors such as strain and octahedral network connectivity[54,55]. Several studies have investigated the relationship between ferroelectric materials and oxygen octahedral structures[56,57]. $BiFeO_3$ has diverse domain structures and exhibits various phase transitions in response to factors such as pressure, temperature, and strain[58-61]. It primarily adopts the rhombohedral *R*3*c* space group with an $a^-a^-a^-$ oxygen octahedral tilt in Glazer notation[62]. The octahedral structure can be altered in various ways through the interfacial connectivity[63,64], resulting in transition between ferroelectricity and antiferroelectricity, and fine-tuned domain spacing[56]. There have also been reports of ferroelectricity induced by variations in the oxygen octahedral structure in materials such as $CaTiO_3$[65]. Similar to most perovskite materials, $CaTiO_3$ adopts the *Pnma* space group, and it exhibits paraelectric properties due to the stable $a^-b^+a^-$ oxygen octahedral rotations, as shown in Figure 3A[66]. It has been shown that local ferroelectricity can emerge at the ferroelastic twin boundaries between antiferroelectric domains in $CaTiO_3$[67,68]; also, ferroelectricity can be induced by the suppression of octahedral distortion when subjected to strong tensile strain[69]. Furthermore, through density functional theory (DFT) calculations, it has been validated that when the oxygen octahedra adopt forms such as $a^-a^-a^-$ or $a^+a^+c^-$, a polar structure can be stabilized, and it realized through the interface engineering[70] [Figure 3B]. This highlights the significant impact that the oxygen octahedral structure can have on the ferroelectric properties of materials.

The delicate rotation of oxygen polyhedral is one of the key parameters to dominate the ferroelectricity in oxides. Brownmillerite structure ($ABO_{2.5}$, A,B = transition metals), as shown in Figure 4A, similar to perovskite structure (ABO_3), has the well-ordered oxygen vacancy channels, leading to the presence of oxygen tetrahedra[71,72]. Brownmillerite has a regularly repeating pattern of oxygen octahedral and tetrahedral layers due to oxygen coordination[73]. In the case of $SrFeO_{2.5}$, a representative brownmillerite structural material, the oxygen octahedral FeO_6 layers are centrosymmetric, similar to the cubic phase of $SrFeO_3$, resulting in a non-polar structure[74,75]. However, the oxygen tetrahedral FeO_4 layers can undergo non-centrosymmetric distortions, leading to ferroelectric properties[76-78]. Interestingly, the oxygen tetrahedra collectively rotate to the left or right in a chain-like manner while also exhibiting displacement. This combined behavior results in ferroelectricity. Theoretically, it has been reported that in $SrCoO_{2.5}$,

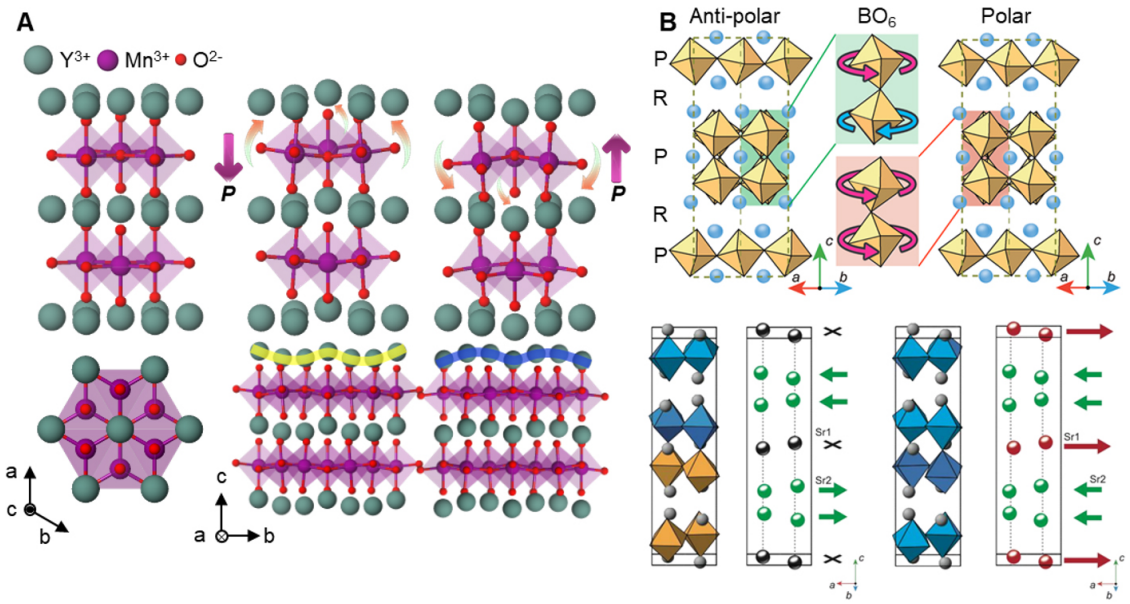

Figure 2. Improper ferroelectric structure with geometric distortion. (A) Hexagonal $YMnO_3$ structure with centrosymmetric non-polar (left), down-polar (middle), and up-polar (right). Distortion of MnO_5 triangular bipyramids is indicated with arrows. (B) Ruddlesden-Popper $Sr_3Zr_2O_7$ layered structures showing polar and anti-polar characteristics. ZrO_6 octahedral rotations determine the polarity of the structure. Reproduced with permission[52]. Copyright 2018, WILEY-VCH Verlag Gmbh & Co. KGaA, Weinheim.

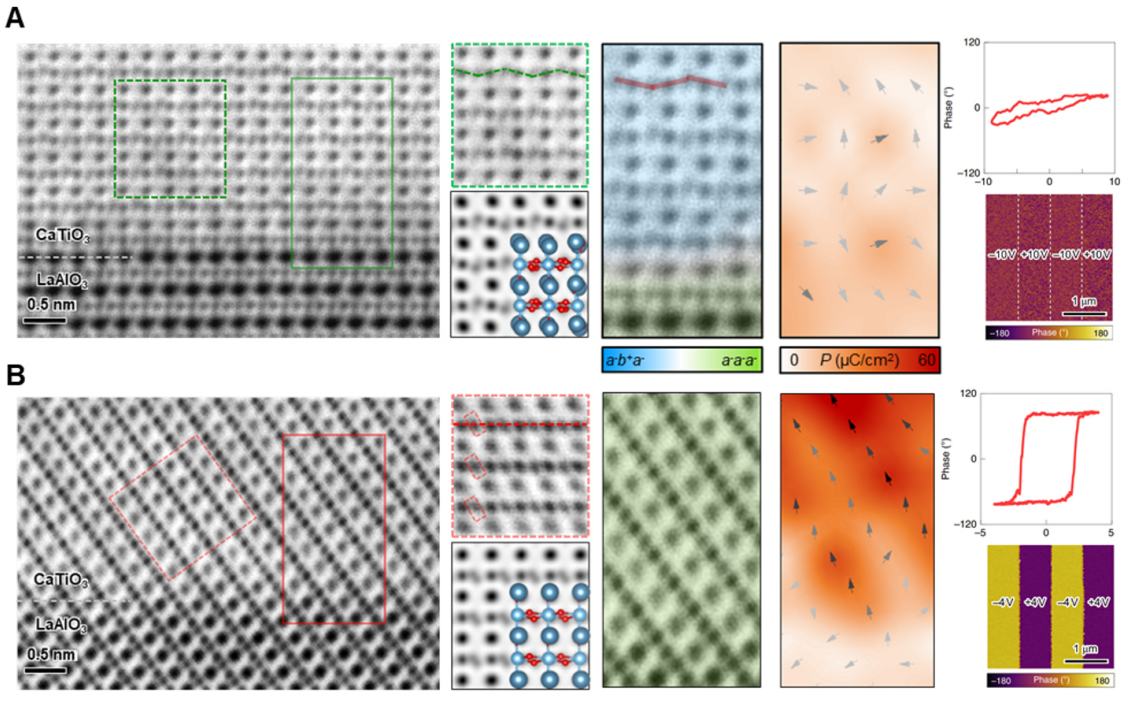

Figure 3. Hidden ferroelectricity of $CaTiO_3$ and oxygen octahedra pattern engineering. (A) Annular bright field (ABF)-STEM and piezoresponse force microscopy (PFM) analysis of paraelectric $CaTiO_3$ on (001) $LaAlO_3$. Corresponding oxygen octahedral rotation mapping and polarization mapping results coincident with the non-polar structure. (B) ABF-STEM and PFM analysis of ferroelectric $CaTiO_3$ on (111) $LaAlO_3$. Corresponding oxygen octahedral rotation mapping, and polarization mapping results coincident with the polar structure. Reproduced with permission[70]. Copyright 2020, The Authors, published by Springer Nature.

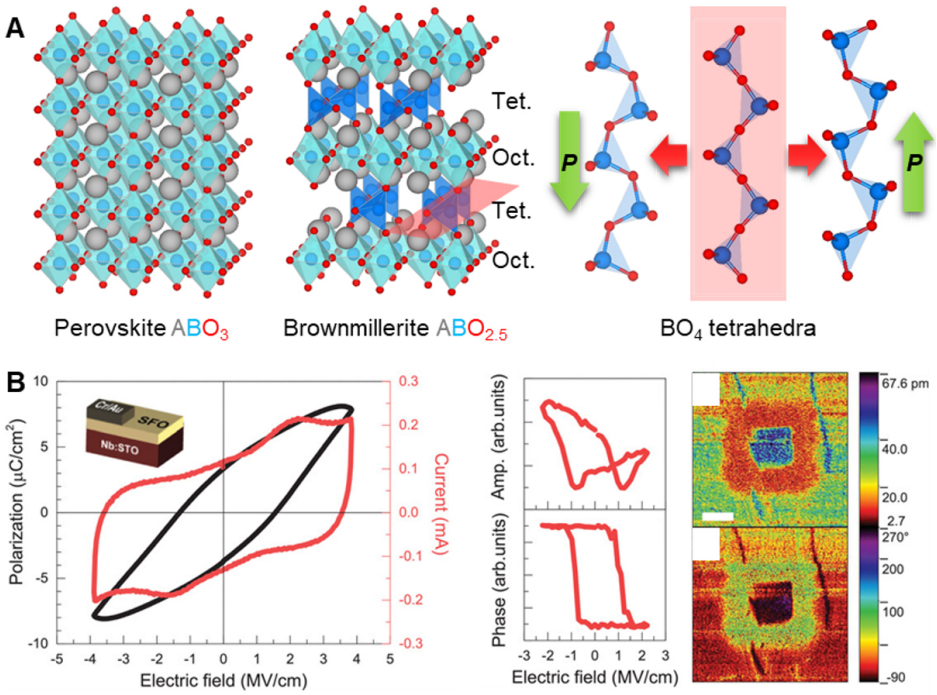

Figure 4. Novel ferroelectricity in brownmillerite structure. (A) Atomic structural features of perovskite and brownmillerite. Tetrahedral chain of brownmillerite can be distorted up and downward. (B) Experimental measurements in brownmillerite $SrFeO_{2.5}$ thin film. Polarization and junction current as a function of electric field (left) and PFM measurements (right). Reproduced with permission[78]. Copyright 2019, WILEY-VCH Verlag Gmbh & Co. KGaA, Weinheim.

depending on the arrangement of the oxygen tetrahedral layer, the Pmc21 space group can be stabilized, leading to the emergence of a ferroelectric state[79]. Furthermore, in the I2bm space group, it has been calculated that the tetrahedral chain rotates in one direction, resulting in a polarization of approximately 6.38 μC/cm²[77]. Experimentally, in $SrFeO_{2.5}$, ferroelectricity has been demonstrated through P-E measurements, second harmonic generation (SHG), piezoresponse force microscopy (PFM), and various other techniques[78] [Figure 4B]. Additionally, the ferromagnetic properties associated with tetrahedral rotation have been observed, confirming its status as a multiferroic material. In the material Bi_2SiO_5, ferroelectricity is induced similarly by the rotation of silicate tetrahedral chains, but there is a difference in that the apical oxygen is fixed in brownmillerite structures such as $SrFeO_{2.5}$[80,81].

Fluorite HfO_2 has a variety of polymorph structures, and depending on the structure, the material can exhibit ferroelectricity. Under ambient temperature and pressure conditions, the monoclinic structure with a non-polar $P2_1/c$ space group is stable in bulk form[82], while it is known to stabilize the metastable non-polar $P4_2/nmc$ tetragonal phase and the polar $Pca2_1$ orthorhombic phase in thin films[16,83,84]. There are many attempts to stabilize this orthorhombic phase through doping or strain. It is known that Si:HfO_2 thin film has a polar orthorhombic structure, which initially nucleates as a metastable tetragonal phase at high temperatures. Depending on the presence or absence of capping during sample cooling, it either becomes a monoclinic phase or stabilizes as a polar orthorhombic phase[15]. In cases where TiN electrode capping is present, mechanical shearing is confined, leading to the manifestation of the orthorhombic structure. This orthorhombic $Pca2_1$ structure has a unique configuration that divides into polar and non-polar layers, gaining attention as a structure that can be ultimately scaled from the perspective of ferroelectric domains and domain walls[85].

FERROELECTRIC DOMAINS

After understanding the structural mechanisms that induce ferroelectricity, when we examine actual ferroelectric material inside, we find the same polarity regions called ferroelectric domains. These domains are separated by interfaces known as domain walls. When polarization is aligned in a single direction, it becomes electrically unstable, prompting the formation of domains to compensate for this instability. In other words, ferroelectric domains result from the interplay between wall energy and depolarization fields induced by surface bound charges from ferroelectric polarization[86]. Ferroelectric domains vary depending on the electrical and mechanical boundary conditions, such as crystallographic orientation, strain, and local defect[87-91]. For instance, in the case of tetragonal proper ferroelectrics such as $Pb(Zr,Ti)O_3$ and $BaTiO_3$, they have polarization in the <001> direction, resulting in domains of 90 and 180 degrees. In contrast, the domains of $BiFeO_3$ have a rhombohedral structure with polarization in the <111> direction, allowing for domains of 71, 109, and 180 degrees[92]. Due to these various angular domains, the vortex nanodomain pattern of $BiFeO_3$, as shown in Figure 5A, has been reported on a $TbScO_3$ substrate[93]. The formation of these domains is driven by localized electrostatic forces, especially at the interface where the 109° domain walls end. Such domains can be switched using an electric field, enabling various applications of ferroelectric materials. Depending on the domain structure, the interaction between domains can either facilitate or hinder switching, potentially influencing parameters such as remnant polarization[94]. In terms of the coercive field, this parameter is related to the effectiveness of domain switching under an electric field[95]. Thus, these parameters can vary depending on the domain structure. For example, HfO_2 possesses a high coercive field, which can be interpreted as a result of the nearly eliminated interactions between domains[85]. Therefore, understanding the domain formations and observing domain motions are essential for the design of practical electronic devices.

Besides, domain walls themselves can present radically different properties from neighboring domains, opening an alternative route towards unusual functionalities with enormous application potential. Because it plays the role of a boundary connecting two domains, lattice distortion is strong[2,96,97], and accordingly, a strain-related driving force arises, making it easy for charged defects to accumulate[98,99]. In the case of $BiFeO_3$ sample grown on $DyScO_3$ substrates with higher deposition rates and with higher oxygen pressure, the 71° domain wall shows small lattice distortion and relatively low conductivity, whereas the 109° and 180° domain walls exhibit significant lattice distortion and high conductivity. In the case of $BiFeO_3$ grown on $SrRuO_3$-buffered $SrTiO_3$ substrates, the conductive nature of a 71° domain wall is also achieved due to oxygen vacancies lowering the Schottky barrier at the domain wall[100]. In addition, when the polarization directions of adjacent domains meet at the domain wall in a tail-to-tail or head-to-head configuration, the charge accumulation results in high metallic conductivity[101-103]. $BiFeO_3$ shows p-type conduction through the appearance of Fe^{4+} and bismuth vacancies at the domain wall[98]. Similarly, in $Pb(Zr,Ti)O_3$, the accumulation of Ti^{3+} at the domain walls enables n-type conduction. In the layered ferroelectric $(Ca,Sr)_3Ti_2O_7$, most of the polarization is aligned in-plane, leading to predominant head-to-head and tail-to-tail configurations and resulting in numerous charged walls[104]. Not only does the domain wall affect conductivity, but it also facilitates the accumulation of oxygen vacancies. This can effectively lower the local energy bandgap, enhance the photocurrent[105], or produce a depolarization field, leading to an increased electromechanical response and, consequently, improved piezoelectric properties[106]. Attempts have been made to utilize the conducting domain wall of $LiNbO_3$ in memristors[107]. These phenomena have triggered efforts to apply domain boundaries in electronic devices for diverse purposes. A $SrRuO_3/BiFeO_3/SrRuO_3$ film was fabricated with a tail-to-tail polarization configuration, inducing in-plane charged domain walls[108]. Using electric field cycling, they demonstrated the ability to create, erase, and move these charged domain walls, revealing memristive characteristics.

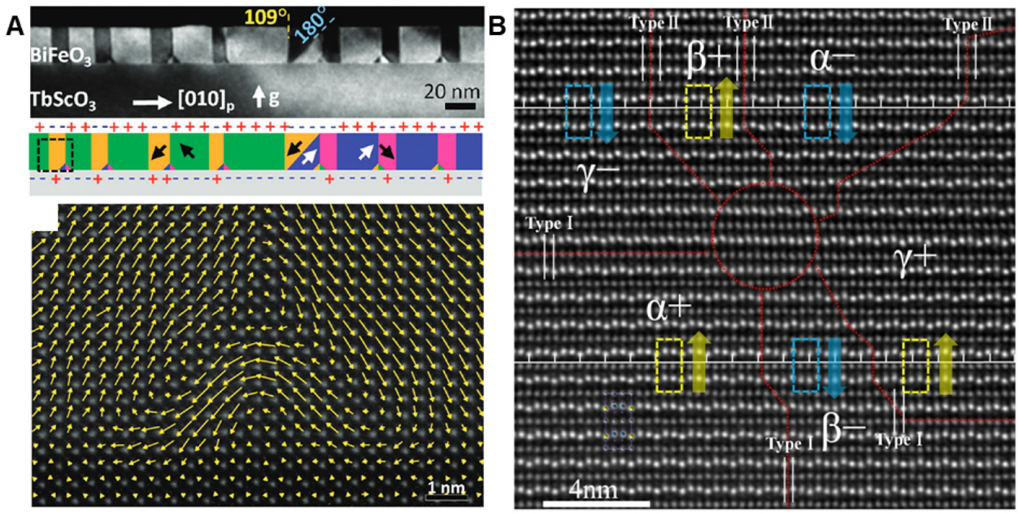

Figure 5. Various types of ferroelectric domains. (A) TEM images of vortex shape nanodomain structure of $BiFeO_3$ thin film. Reproduced with permission[93]. Copyright 2011, American Chemical Society (B) Atomic scale STEM image of small size of domains in improper ferroelectric, $YMnO_3$. Reproduced with permission[96]. Copyright 2013, The Authors, published by Springer Nature.

In the improper ferroelectric $YMnO_3$, the ferroelectric domain is interestingly coupled with magnetic order[109], making its domain structure different from conventional ferroelectrics. $YMnO_3$ can exhibit six distinct domain patterns[96,110,111] [Figure 5B]. Structural distortions at domain walls, accompanied by Y ion movements, manifest as antiphase boundaries combined with ferroelectric domain walls. Considering a domain labeled as α as the baseline structure, α, β, and γ domains exhibit antiphase boundary relationships. With polarization directions denoted as + or -, a total of six possible domains can emerge from a single point, forming a cloverleaf pattern. These domains appear periodically as α, β, γ and can be defined as either clockwise or anti-clockwise vortex directions based on their order. While enhanced conductivity observed in domain walls of materials such as $BiFeO_3$ and $Pb(Zr,Ti)O_3$ was not evident in $YMnO_3$'s conductive atomic force microscopy (c-AFM) results[110], there are findings of domain wall conductivity due to vacancy ordering in oxygen-deficient situations[112]. However, the domain orientation in $YMnO_3$ can vary, being either in-plane or out-of-plane[113]. Depending on how domain walls meet, they can exhibit characteristics of charged domain walls in the case of tail-to-tail longitudinal domain walls or uncharged domain walls when forming antiparallel transverse domain walls[51,114].

In Y-doped HfO_2 single crystals, the structure stabilizes from monoclinic to orthorhombic based on the yttrium doping concentration[115]. With about 12% doping, a stable ferroelectric domain with 90° and 180° domains was imaged. However, in thin films, a mix of various structures such as monoclinic, orthorhombic, and tetragonal is commonly observed, intertwined in small-sized grains with varied orientations, necessitating atomic scale analysis using STEM. HfO_2 thin film is known for its wake-up effect, where the structure changes and domains align under an electric field, enhancing its ferroelectric properties[116]. For instance, in a Gd-doped HfO_2 film, the monoclinic, orthorhombic, and tetragonal structures coexist as nanosized grains[117] [Figure 6A and B]. The 90° domain boundaries of the orthorhombic structure are displayed similarly to those in Figure 6C; however, after field cycling, switching occurs at the 90° domain wall. Similarly, in $Hf_{0.5}Zr_{0.5}O_2$, both uncharged and negatively charged types of 90° domain walls were identified, and it was revealed through field-cycling that a 90° domain wall transforms into a 180° domain wall. This was used to explain the origin of the wake-up effect. Computational studies on the domain forms of HfO_2 ferroelectric orthorhombic structure revealed various domain wall formations depending on polarization orientation and lattice matching. Notably, a specific 180° domain wall energy showed a

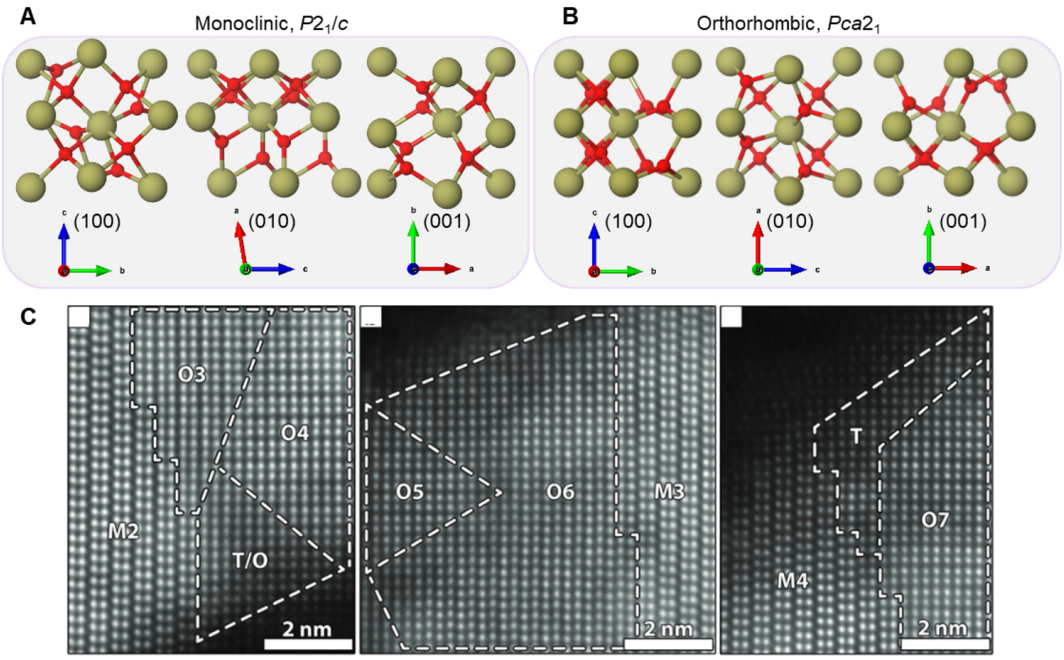

Figure 6. Polymorphic domain structure of HfO_2. (A) Monoclinic atomic structures with three different directions. (B) Orthorhombic atomic structures with three different directions. (C) HAADF-STEM images show intermixed monoclinic and orthorhombic, and tetragonal structure with a few nanometer scales. Reproduced with permission[117]. Copyright 2018, WILEY-VCH Verlag Gmbh & Co. KGaA, Weinheim.

negative value of about 21.3 mJ/m^2, indicating stabilization of an anti-polar domain[118]. These findings pave the way for future studies on ultranarrow domains that maintain polarization at a half-unit cell width and on scaled-down ferroelectrics[85].

Beyond the domain walls in ferroelectrics, exotic topological domain structures have become a significant research focus[119]. As the dimensions of ferroelectrics decrease, the influence of boundaries such as interfaces and surfaces increases, leading to the formation of structures such as flux-closure domains[120], polar vortices[121], skyrmions[122], merons[123], and hopfions[124] [Figure 7A]. These structures, studied extensively in magnetic materials, pose a challenge in ferroelectrics due to the strong coupling between the lattice and polarization. This coupling causes an energy penalty for polarization rotation against the crystallographically permitted directions, making the creation of exotic topological structures more challenging than in magnetic materials. However, advancements in theoretical studies and experimental characterization methods have spurred research into various topological structures. Theoretical studies on new topological polar vortices in reduced dimensions, such as nanodots and nanorods, have led to numerous investigations[125,126]. For instance, when $PbTiO_3/SrTiO_3$ multilayer films are grown under tensile strain on $GdScO_3$, flux-closure domains form, as shown in Figure 7B, with their periodicity varying with the thickness of the $PbTiO_3$ film[120]. These structures emerge as a result of the interplay between elastic energy, electrostatic energy, and polarization gradient energy. In superlattice $PbTiO_3/SrTiO_3$ on $DyScO_3$, for example, the formation of polar vortices is driven by competition among the epitaxial constraint-induced elastic energy in $PbTiO_3$ on $DyScO_3$[121], the significant polar discontinuity between $PbTiO_3$ and $SrTiO_3$ causing electrostatic energy, and the gradient energy required for changes in polarization direction and magnitude. Factors such as the periodicity of the superlattice and strain play a crucial role in this competition. For periodicity shorter than ten unit cells, conventional a_1 and a_2 domains form, whereas longer periodicities lead to the formation of flux-closure domains. In addition, on TiO_2-terminated $SrTiO_3$

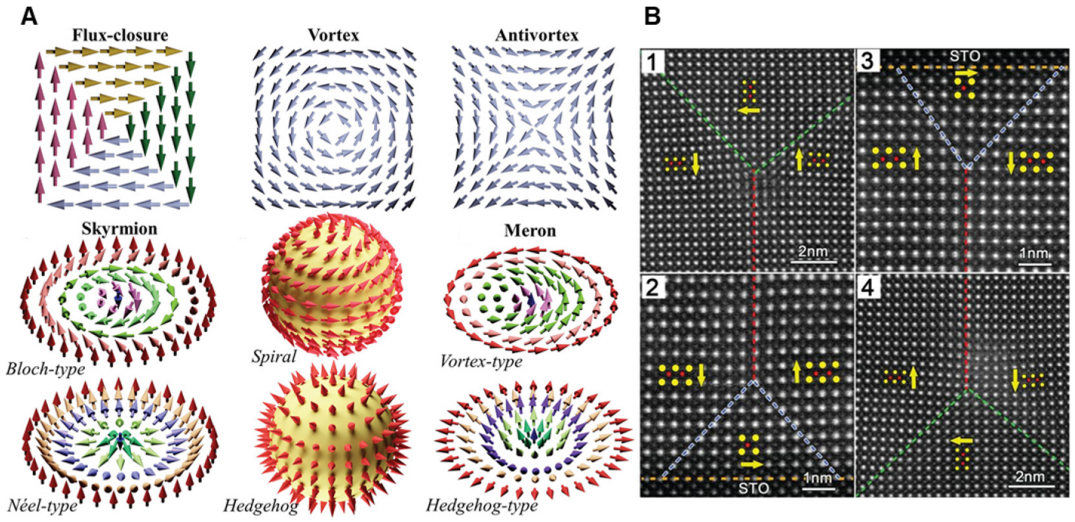

Figure 7. Exotic topological ferroelectric domains. (A) Representative examples of topological structures. Each arrow indicates the direction of polarization. Reproduced with permission[119]. Copyright 2020, Wiley-VCH Gmbh. (B) Atomic scale STEM image of flux-closure domains in $PbTiO_3/SrTiO_3$ multilayer films. Reproduced with permission. Yellow arrows represent the directions of polarization. Reproduced with permission[120]. Copyright 2015, American Association for the Advancement of Science.

substrate, which imposes compressive strain as opposed to the tensile strain of $DyScO_3$, polar skyrmions can be obtained. When a 5 nm $PbTiO_3$ film is grown on $SmScO_3$ substrate under tensile strain, polar merons, which are akin to half-formed skyrmions, are observed. These exotic topological structures hold potential for applications in advanced memory devices and nanoelectronics.

FILM THICKNESS SCALING

In thin films, the characteristics of the material can differ significantly from bulk due to the size effect, notably effects caused by strain, interfaces, *etc*. Consequently, the form of domains can change, and the overall characteristics of the thin film can be entirely different. For example, strained $BaTiO_3$ thin films grown on $DyScO_3$ and $GdScO_3$ substrates lead to enhanced ferroelectric properties[127]. Ferroelectric transition temperature is almost 500 °C higher, and a remnant polarization is at least 250% higher than bulk $BaTiO_3$ single crystal. In thin films of paraelectric $SrTiO_3$, ferroelectricity can be realized at a thickness of fewer than 12 unit cells due to polar nanoregions induced by antisite defects[13], as shown in Figure 8. For another paraelectric $CaTiO_3$, when thin film growth is induced in the (111) direction, ferroelectric structural characteristics appear up to about 9 nm, and beyond that, the original *Pnma* phase paraelectric characteristics appear[128].

With the advancement of various thin film synthesis methods such as pulsed laser deposition (PLD), molecular beam epitaxy (MBE), and atomic layer deposition (ALD), it became possible to deposit ferroelectric materials very thinly, enabling the development of miniaturized ferroelectric materials with newly induced ferroelectric properties. However, ferroelectricity in thin films does not always appear favorably[129]. In terms of a dead layer, a parasitic low permittivity layer associated with the boundary between ferroelectric and electrode, it is thought to cause a collapse in the permittivity of thin film capacitor structures. This limits the effective use and integration of high permittivity materials. While the dead layer is an inherent feature at the dielectric-metal interface, it can be engineered out in certain cases, particularly where interface bonding is weak. For $SrTiO_3$ single crystals, theoretical analyses have confirmed the presence of a dead layer, predicting strong intrinsic suppression of permittivity[130]. Experimentally, when lamellae of $SrTiO_3$ single crystals, created using a focused ion beam (FIB), are formed into capacitor

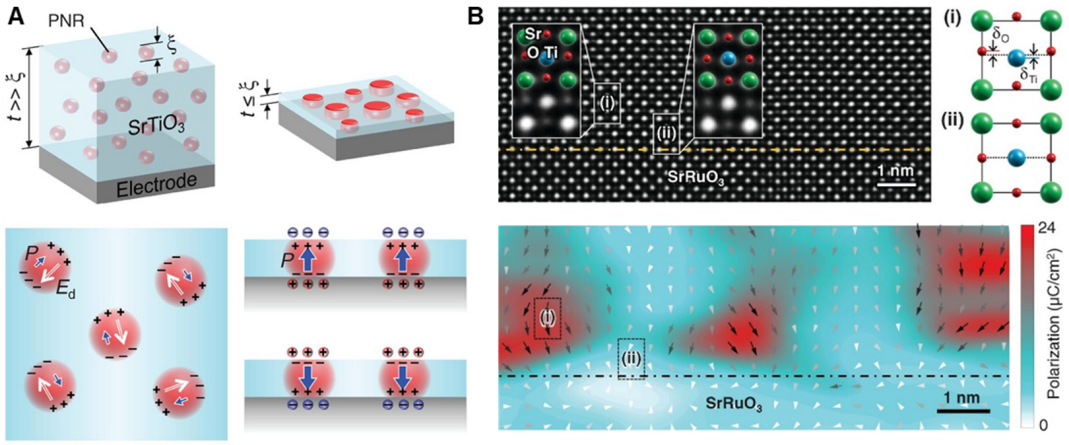

Figure 8. Emergence of ferroelectricity in ultrathin films of otherwise non-ferroelectric $SrTiO_3$. (A) Schematics illustrating the effect of polar nanoregions based on thickness. In thicker films, polar nanoregions are not effectively aligned, whereas in thinner films, they align well. (B) Inverted ABF-STEM image and corresponding polarization mapping. Polar nanoregions are well visualized. Reproduced with permission[13]. Copyright 2015, American Association for the Advancement of Science.

structures with Pt electrodes, a significant inherent suppression of permittivity is observed, despite $SrTiO_3$ remaining intact up to the interface[131]. However, in specific systems, this dead layer can be eliminated. For example, in $BaTiO_3$ single crystals made into lamellae and constructed into an Au/$BaTiO_3$/Au structure, there are no indications of permittivity suppression in thin films as thin as 75 nm[132]. This indicates the possibility of engineering out the dead layer by controlling defects and strain. Theoretical calculations have revealed the potential existence of a negative dead layer in ferroelectric capacitors, especially when proper interface termination is established[133]. This understanding not only confirms the existence of strong intrinsic effects even with perfect interfaces but also emphasizes that with an appropriate choice of electrode material, interface bonding effects can enhance the dielectric response, overcoming the material's limitations. This understanding confirms strong intrinsic effects even in perfect interfaces and highlights the importance of selecting suitable electrode materials, thereby overcoming the inherent limitations of the materials.

Also, ferroelectric materials inherently have a size effect, where ferroelectricity decreases as the critical thickness is approached. This phenomenon has been a significant topic of discussion. In reality, the limit of critical thickness exists due to factors such as defects and interface effects within materials. As the film becomes thinner, the effect of the depolarization field increases[134], and with increased interface, issues arise from oxygen vacancy and charge injection at the interface between metal electrodes and ferroelectrics, leading to fatigue after cycling, reducing endurance. In recent years, many studies on thin films have been conducted to overcome the limitations of critical thickness. Several materials and their critical thickness and polarization characteristics are introduced. It has been confirmed that a (001) oriented $BaTiO_3$ thin film between two metallic $SrRuO_3$ electrodes shows ferroelectricity down to a thickness of about six unit cells[134]. The disappearance of ferroelectric instability is due to a depolarizing electrostatic field, which arises from dipoles at the ferroelectric-metal interfaces. It is also evident that the softness of the $SrRuO_3$ lattice plays a pivotal role in screening the ferroelectric polarization in $BaTiO_3$. The critical thickness for ferroelectricity is further reduced to 1.2 nm[135]. For $Pb(Zr,Ti)O_3$, a critical thickness as thin as that of $BaTiO_3$ has been reported[11]. In $PbTiO_3$ thin films with a stripe domain pattern, a study revealed the correlation between the reduction in film thickness and the decrease in Curie temperature[136]. Based on these findings and subsequent calculations, it was predicted that films as thin as two unit cells could be formed at lower temperatures. Using synchrotron X-ray, it has been demonstrated that at room temperature, the

ferroelectric critical thickness can be reduced to as little as three unit cells, about 1.2 nm[11]. There was even a subsequent report suggesting an absence of critical thickness altogether[137]. Through STEM analysis, films grown on $SrTiO_3$ with a $SrRuO_3$ electrode showed a remnant polarization of 22 μC/cm² down to a two unit cells thickness. In contrast, films grown on $SrTiO_3$ without a $SrRuO_3$ electrode exhibited a reduced polarization of 16 μC/cm² at a mere 1.5 unit cells (0.6 nm) thickness, as shown in Figure 9. In the case of $BiFeO_3$, although the bulk is rhombohedral, thin films can stabilize in a tetragonal structure due to strain[138]. Several reports showed that ferroelectricity appeared in such thin films in a tetragonal phase[139]. When transformed to a tetrahedral-like structure on a $La_{0.7}Sr_{0.3}MnO_3$ bottom electrode, strong out-of-plane polarization was reported to appear even at a thickness of 1.2 nm due to the accumulation of oxygen vacancies at the interface. Furthermore, at room temperature, tetragonal phase $BiFeO_3$ on an $SrRuO_3$ electrode was reported to have robust out-of-plane spontaneous polarization even at one unit cell thickness[140]. Although very thin, compared to bulk, the polarization characteristics themselves were significantly degraded, so this trade-off needs to be addressed.

For the improper ferroelectric $YMnO_3$, it was reported through calculations that there might be no critical thickness[141]. The intrinsic bulk polarization is 8.7 μC/cm², smaller than conventional proper ferroelectrics, but in films, it is slightly smaller at 6.5 μC/cm². It is known that it can have a single domain without electrodes or external fields, unlike proper ferroelectrics in terms of free energy. This polar state has been experimentally proven through STEM and SHG, and it was maintained even at a thickness of three unit cells, about 10 nm[142]. At a very low temperature of 20 K, it was confirmed that hexagonal $YbFeO_3$ had no critical thickness limit up to three unit cells[143]. Especially through the fitting of depolarization effects, it was proven that the spontaneous polarization was maintained even as the thickness became very thin. In layered bismuth oxide Sm-substituted Bi_6O_9, ferroelectric properties were found even at a thickness of less than one nanometer at room temperature[144]. In particular, it was confirmed that the remnant polarization has a high value of 17 μC/cm², even at a reduced thickness [Figure 10].

HfO_2 shows promise for polarization-driven memories and ferroelectric-based transistors because of their compatibility with complementary-metal-oxide-semiconductor technology. When ferroelectricity was first reported in Si:HfO_2 thin films with a thickness of 10 nm, it was expected that they would exhibit high ferroelectricity even at thin thicknesses[15]. In the case of $Hf_{0.5}Zr_{0.5}O_2$ grown on the metallic pyrochlore $Pb_2Ir_2O_7$, the polar orthorhombic phase stabilizes at thicknesses below 30 nm, and ferroelectric characteristics were confirmed even at 5 nm[145]. Near the interface, the orthorhombic phase remains stable, while in thicker films, the upper portion transitions into a non-polar monoclinic phase with a finger-like shape. A 10 nm thick Y:HfO_2 grown in the (111) direction was reported to have a very large polarization value of 64 μC/cm²[146]. When oriented in the (111) direction, the $Pca2_1$ orthorhombic phase becomes stable, exhibiting minor rhombohedral distortion, which highlights the significance of structural limitations in maintaining the ferroelectric phase. Ferroelectricity was confirmed in $Hf_{0.5}Zr_{0.5}O_2$ grown by ALD, even at an incredibly thin thickness of 1 nm[147]. From a structural perspective, as the material's size decreases, it undergoes structural distortion and shifts towards higher symmetry. Unlike conventional perovskite structures that transition to non-polar, the fluorite-structured $Hf_{0.5}Zr_{0.5}O_2$ exhibits a high-symmetry polar orthorhombic phase rather than a non-polar monoclinic one. As a result, ferroelectricity increases with decreasing size. Similarly, ZrO_2, possessing the same fluorite structure, typically remains stable in the antiferroelectric tetragonal phase[148]. However, when its thickness is reduced to 2 nm or less, it transitions to the ferroelectric $Pca2_1$ orthorhombic structure. Notably, ferroelectric properties persist even at a unit cell thickness as thin as five angstroms.

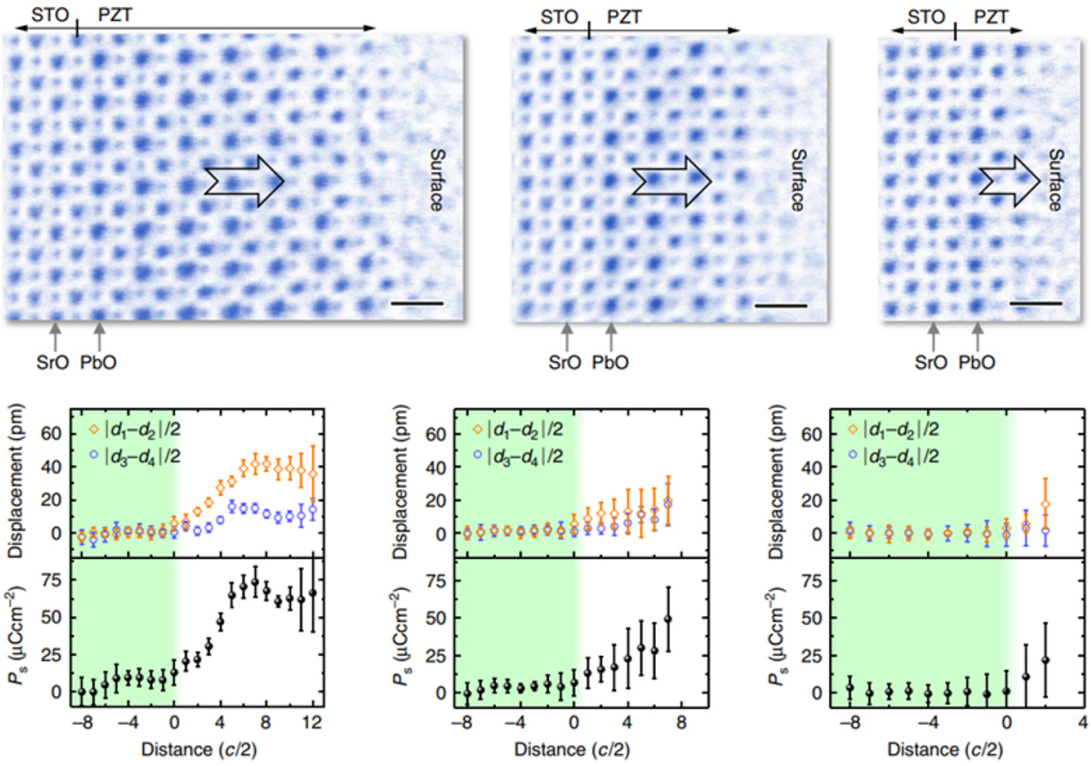

Figure 9. Thickness-dependent ferroelectricity in $Pb(Zr,Ti)O_3$ on a $SrTiO_3$ substrate. ABF images from regions with thicknesses of 6.5, 4, and 1.5 unit cells. Displacements and polarizations consider both the cation and oxygen. While polarization is suppressed in thin film, it remains stable. Reproduced with permission[137]. Copyright 2017, The Authors, published by Springer Nature.

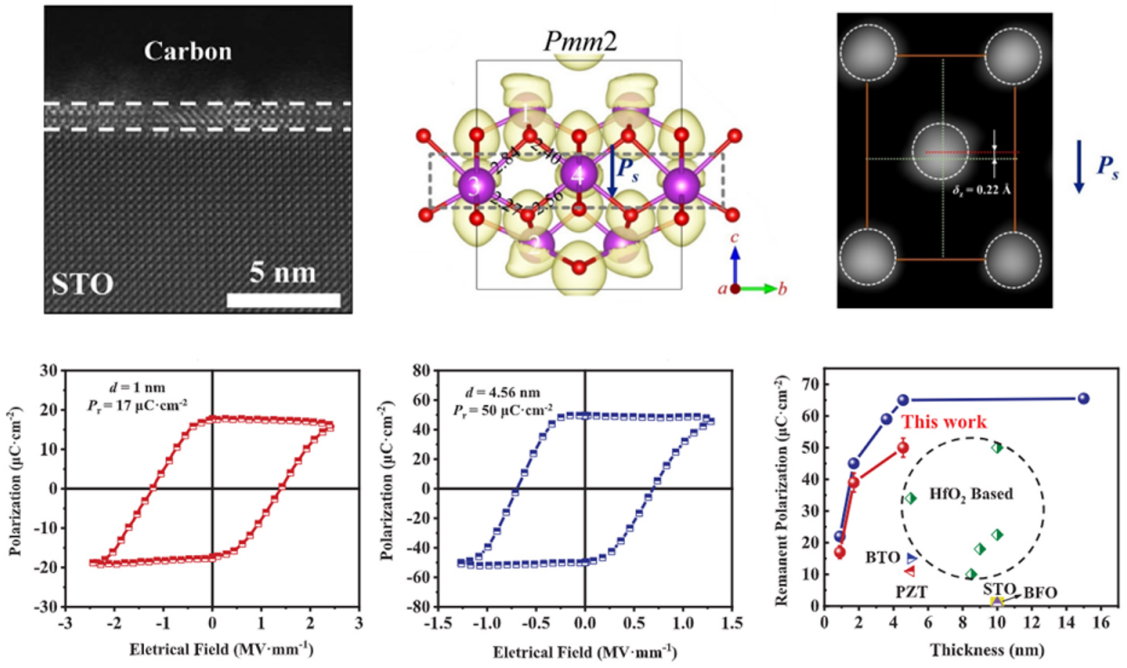

Figure 10. Ferroelectricity in layered bismuth oxide. The HAADF-STEM image shows a well-grown film with a thickness of one nanometer. Despite the film being reduced by 1 nm in thickness, the remnant polarization remains high. Reproduced with permission[144]. Copyright 2023, The Authors, some rights reserved; exclusive licensee American Association for the Advancement of Science.

FERROELECTRIC DOMAIN WIDTH SCALING

For high-density integration, it becomes extremely important to not only reduce the thickness of the ferroelectric thin film but also downsize the width of the domain, which serves as an information unit. In terms of domain size, it is classically described by the Landau-Lifshitz-Kittel's law concerning ferroic domains[149-151]. This law was theoretically proposed based on a straightforward stripe-patterned domain. As the domain's vertical dimension area grows, the energy of the domain wall also increases. Consequently, when the thickness increases, the formation of a domain wall is avoided, leading to a larger domain size. Moreover, when the domain's volume energy decreases, its formation becomes more stable. This relationship can be mathematically represented by the square root dependence on the domain size's thickness. Initially, this law was introduced to describe the domain of ferromagnetism. However, Mitsui and Furuichi later extended it to the ferroelectric Rochelle salt 180° domain structure[86]. In the case of single crystal $BaTiO_3$, lamellae were created using a FIB to observe domain changes according to thickness[152]. This approach demonstrated, through direct STEM observation, that the law governing these changes applies well from the millimeter scale down to the nanometer scale. In addition, within a single lamella, it was observed that a sharp thickness gradient leads to a strong bifurcation. In the context of thin films, the relationship is direct: an increase in film thickness results in a larger domain size, while a decrease leads to a smaller domain size. In $PbTiO_3$ thin films, a nanoscale 180° stripe domain pattern was confirmed as a satellite pattern in X-ray scattering[136]. It was observed that as the thickness reduced to 1.6 nm, the periodicity of these domains decreased to as small as 3.7 nm. Also, this has been observed in $Pb(Zr,Ti)O_3$ films, where changes in the size of the stripe pattern's a-domain with respect to thickness were confirmed using PFM and TEM. The critical thickness for forming a stripe pattern was found to be around 60 nm, and the domain width was constrained to approximately 10 nm at that thickness[153].

Another issue causing small-sized domains is the thickness of the ferroelectric domain wall. Ferroelectricity naturally creates domains with Ising-, Bloch-, or Neel-type domain walls to prevent sudden polarity shifts, which can often weaken the magnitude and confined size of ferroelectricity [Figure 11A]. Neel-like domain walls have been observed in $Pb(Zr,Ti)O_3$ single crystals and thin films, while Bloch-type domain walls were observed in $LiTaO_3$ single crystals[154-156]. In such domain walls, to change the aspect of polarization, the size must either diminish or the polarization must decrease through rotation, as shown in Figure 11B. Consequently, the thickness of the domain wall is large, and the domain size is limited. Moreover, because ferroelectricity is influenced by the soft phonon mode, which represents a collective movement of atom displacements, the switching scale of individual domains is inherently restricted[85].

For the improper ferroelectric hexagonal $ErMnO_3$, the situation is somewhat similar. At specific local domain wall points, very thin domains with a thickness of one unit-cell have been observed, which was attributed to strong electrostatic attractive interactions[157]. However, this was not a commonly observed feature. Due to the coexistence of the general antiphase boundary and the ferroelectric domain wall, there are limitations to the wall width. In $ErMnO_3$, the thickness of the ferroelectric domain wall is around a few nanometers, with observations showing a gradual switch in polarization[158,159].

Pca2_1 orthorhombic HfO_2 has garnered significant attention due to its remarkably fine domains and walls with a half-unit cell width[85] [Figure 11C]. The domain formation in HfO_2 stems from the alternating arrangement of ferroelectric and spacer layers, leading to a flattened phonon dispersion. As a result, HfO_2 can switch via the creation of zero-width domain walls, contrasting the diffused domain walls observed in prototypical ferroelectric $PbTiO_3$. Analysis of STEM images for $PbTiO_3$ reveals these diffused domain walls, where a reduction in the strength of polarization is noticeable over a domain wall area spanning 1~3 nm, accompanied by lattice distortion[155]. In contrast, the half-unit cell domain width of HfO_2 was directly

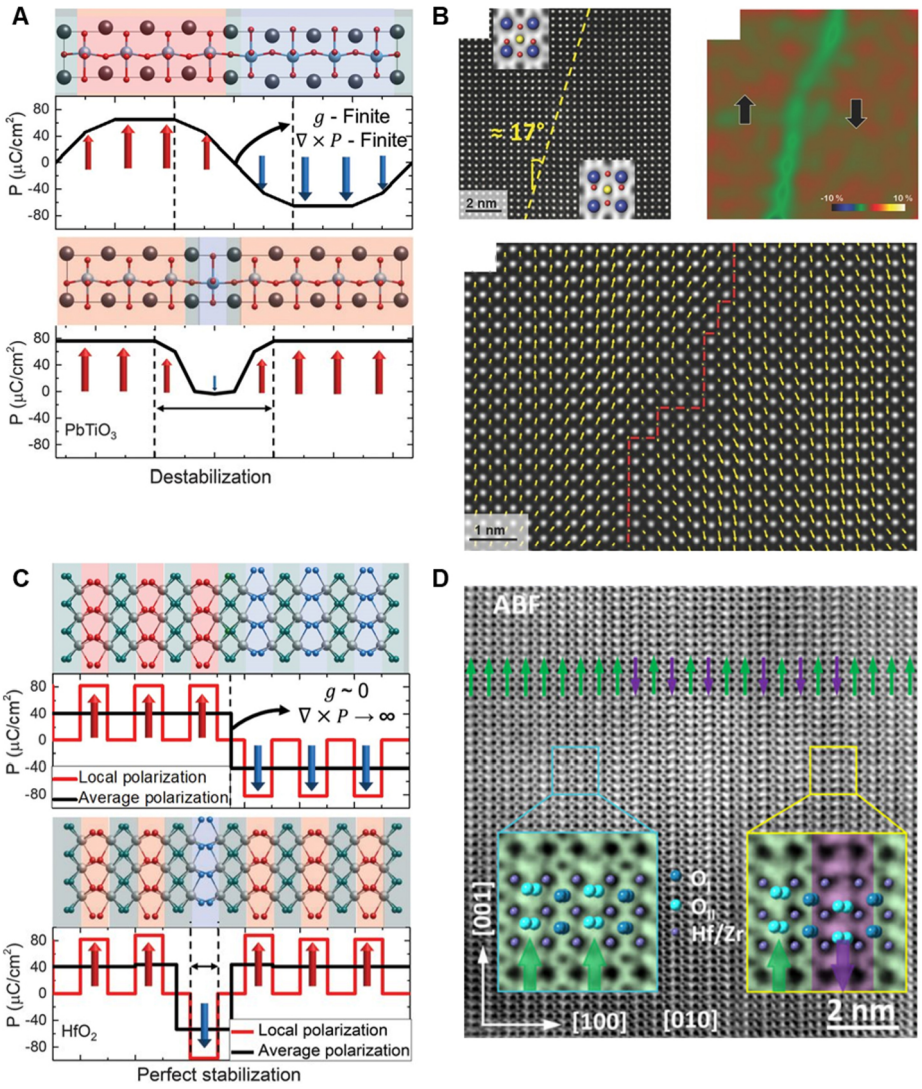

Figure 11. Scaling of domain wall width in $PbTiO_3$ and HfO_2. (A) Calculation results of the finite thickness of the domain alongside the destabilized one unit cell-width domain. (B) HAADF-STEM images of Neel-like domain wall in $Pb(Zr,Ti)O_3$. Reproduced with permission[155]. Copyright 2016, WILEY-VCH Verlag Gmbh & Co. KGaA, Weinheim. (C) Calculation results of zero-width domain wall and stabilized on unit cell-width domain. (D) ABF-STEM image of the unit cell-width domains in HfO_2. (A and C) Reproduced with permission[85]. Copyright 2020, The Authors, some rights reserved; exclusive licensee American Association for the Advancement of Science. (D) Reproduced with permission[14]. Copyright 2022, The Authors, published by Springer Nature.

verified in $Hf_{0.5}Zr_{0.5}O_2$ films grown between TiN electrodes using STEM [Figure 11D]. Polarization in HfO_2 manifests solely within the polar layers, with the movement of oxygen in the Hf lattice confirming this polarization. In the as-grown state, domains with unidirectionally aligned polarization are visible on the left of Figure 11D, while those with alternately aligned polarization appear on the right of Figure 11D. Unique oxygen displacement configurations, such as down-up-up-down-up, have been observed, and these structural attributes vividly depict the zero-width domain wall characteristics[14].

Another example of ultrafine domains is $CsBiNb_2O_7$[19] [Figure 12A]. This material, with its layered Dion-Jacobson phase, can be exfoliated in a quasi-two-dimensional manner due to the weak bonding between layers. The in-plane polarization, aligned in the layer direction in the bulk crystal state, can exhibit unit cell-sized domains. This characteristic is attributed to the Cs ion weakening the bond between the NbO_6

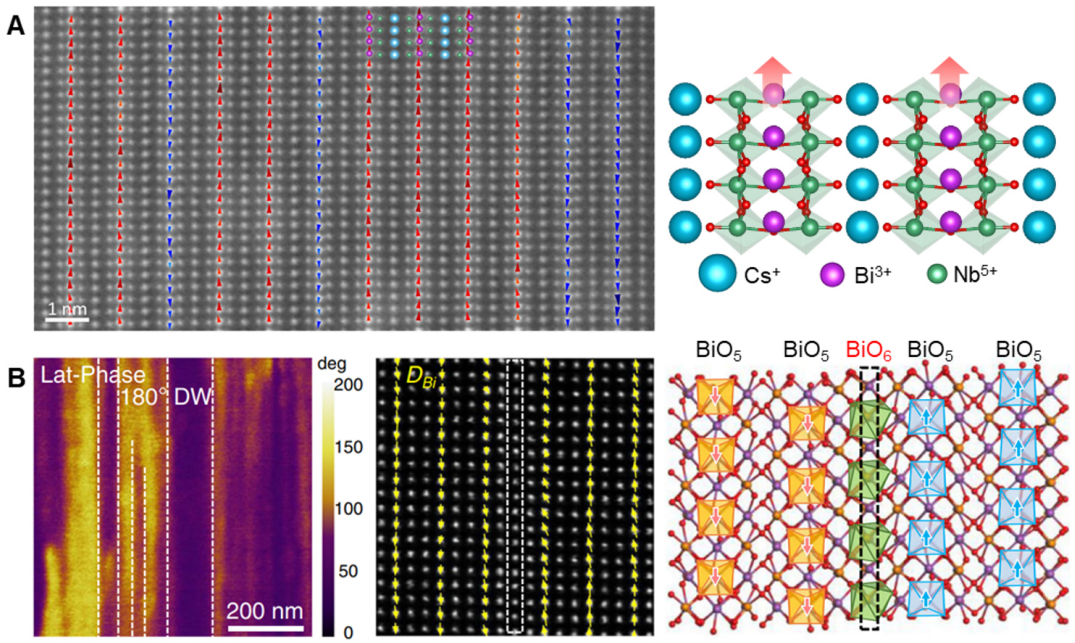

Figure 12. Unit cell-width ferroelectricity in various materials. (A) HAADF-STEM image and atomic structure of layered $CsBiNb_2O_7$. Displacements of Bi ions are indicated by arrows. Reproduced with permission[19]. Copyright 2021, American Physical Society. (B) PFM and HAADF-STEM images accompanied by the atomic structure. When domain walls form, BiO_6 octahedra emerge. Reproduced with permission[160]. Copyright 2022, The Authors, published by Springer Nature.

octahedra layers, resulting in reduced domain wall energy. In HfO_2, the polar and spacer layers have different oxygen coordination numbers, three and four, respectively, and each layer exhibits very weak coupling, preventing lattice vibrations from propagating. Likewise, layered perovskites show weak couplings between oxygen polyhedra across each layer, suggesting a possible origin for layer-resolved ferroelectricity. Bi_2TeO_5 is another example where unit cell-wide domains form due to weakened connections between oxygen polyhedra[160] [Figure 12B]. Bi_2TeO_5 has a layered structure primarily consisting of pyramidal BiO_5 pentahedra. When a domain boundary forms, an additional BiO_6 octahedron intercalates as a buffer layer between the adjacent polar BiO_5 layers, reducing domain wall energy. These examples illustrate that weakened connectivity in the oxygen polyhedral network is a key factor in inducing unit cell-wide ferroelectric domains.

The brownmillerite material is of interest when examining unit cell-wide domains. What makes it unique is its structure: it alternates between oxygen octahedra and oxygen tetrahedra, with a distinctive arrangement of oxygen vacancy channels[161]. Interestingly, only the oxygen tetrahedra exhibit ferroelectric properties in brownmillerite, whereas the oxygen octahedra remain non-polar[162]. This alternating structure, with non-polar regions disrupting the continuity of polar regions, is a trait also seen in other materials such as HfO_2, $CsBiNb_2O_7$, and Bi_2TeO_5. Specific types of brownmillerite, namely $CaFeO_{2.5}$ and $SrFeO_{2.5}$, have unique structures: the former is anti-polar, and the latter is polar. If these polarizations were to intermix, they might display a random polarization pattern akin to the sequence observed in HfO_2.

CHARACTERIZATION TECHNIQUES FOR FERROELECTRICS

Beyond the measurements of polarization-electric field or polarization-voltage hysteresis, which validate fundamental traits of ferroelectrics such as spontaneous and remnant polarization and the coercive field, there is a need to study the structural features and switching behaviors of ferroelectric domains for their

integration into electronic devices. Microscopy-based imaging methods are predominantly used to evaluate these characteristics. At its simplest, domains are visualized using an optical microscope that employs polarized light. This approach is non-destructive and primarily captures domain patterns that are a micrometer in size or larger. As the trend moves towards smaller electronic devices, the spotlight has turned to techniques such as X-ray imaging, scanning probe microscopy (SPM) imaging with nanometer-scale probes, and TEM imaging on the unit cell level[163-166]. Every method brings its unique strengths and challenges, and often, a combination of techniques is employed to elucidate ferroelectric properties. This review seeks to delve into the TEM imaging approach, focusing on the detailed examination of miniaturized domains and their related atomic structures. In this section, we will discuss the TEM imaging method, emphasizing a detailed exploration of miniaturized domains and recent advancements in the atomic-level structures.

Before discussing the TEM imaging approach, it is worth noting that PFM is a powerful tool for investigating the domain dynamics of ferroelectrics[167]. The principle of PFM involves using the piezoresponse force, which acts between the scanning probe and the surface of the sample while scanning the surface with the probe[168]. The contrast of the domain is due to the converse piezoelectric effect induced by AC voltage, resulting in a topographic image. PFM allows for nondestructive visualization and control of ferroelectric domains, not only sensing with the probe but also directly applying bias to facilitate domain switching, making it an excellent method for observing domain wall motion[169]. The resolution in PFM is determined by the size of the scanning probe's apex, with recent advancements achieving imaging resolution down to about 10 nm from the micrometer level. Advanced PFM offers a range of versatile modes, such as switching spectroscopy PFM that captures local hysteresis loops at individual points[170], Stroboscopic PFM for nanosecond time resolution[171], resonance-enhanced PFM to boost measurement sensitivity[172], along with dual AC resonance tracking PFM[173], and band-excitation PFM[174].

To analyze the precise atomic structure of ferroelectrics, TEM serves as a powerful observation tool enabling atomic scale examination with the use of a short-wavelength electron beam. The transmitted beam interferes with the ultra-thin specimen, generating phase information about the periodic crystal structure. Crystallographic information and chemical composition can be characterized using TEM. In addition, TEM is suitable for identifying the domain structure over a relatively large area, spanning a few square micrometers. In particular, dark-field TEM images, which select specific diffraction spots, show a strong bright contrast for the selected region under a two-beam condition. Because diffraction spots can violate Friedel's law based on the polarity of the structure, ferroelectric domains are distinctly visualized by intensity in dark-field TEM. Furthermore, TEM operates in real-time mode, enabling *in situ* imaging under conditions such as the application of an electric field or heating, and it also offers the advantage of visualizing defects in materials and polymorphic structures[175].

Using *in situ* holders, a conductive nanoprobe is precisely positioned to contact the specimen through a piezo-driven manipulator[176]. The ferroelectric switching process can be observed *in situ* with this nanoprobe, as demonstrated in a $Pb(Zr,Ti)O_3$ thin film[177,178]. The intrinsic electric fields, established at the interfaces between the ferroelectric and electrode, dictate the nucleation sites and growth rates of the ferroelectric domains, as well as the orientation and mobility of domain walls. Meanwhile, dislocations exert only a mild pinning force on the movement of domain walls. In a capacitor configuration using a $Pb(Zr,Ti)O_3$ film between Ni and $SrRuO_3$ electrode, a ferroelectric hysteresis graph resembling the typical P-E hysteresis is derived from the switched area-electric field curve[179]. In a study concerning $Pb(Mg_{1/3}Nb_{2/3})O_3$-0.38$PbTiO_3$ (PMN-PT), the influence of electric field on ferroelectricity was explored based on the thickness of the TEM sample[180]. The results demonstrated that, for thicker samples, the 90-

degree domain switches to 180 degrees when subjected to electric biasing. In contrast, thinner samples maintained the 90° domain [Figure 13]. Given that TEM samples need to be exceptionally thin to permit electron beam transmission, their characteristics, when thin, are distinct from those of thicker counterparts, providing a clear insight into domain behavior at a reduced scale.

Although most research has been focused on studies using conductive nanoprobes, recent experiments have been conducted using micro-electromechanical systems (MEMS) devices to apply electric biasing locally and stably[181,182]. Ferroelectric thin film samples are usually prepared by creating a lamella using FIB and then transferring the sample[181,183]. Through the design of the sample's electrode, the electrical path can be constructed as desired, either in-plane or out-of-plane[182,184,185]. In PMN-PT single crystal, electrical biasing experiments were conducted using a MEMS chip. During the 280 electrical cycles, c-domain formation was observed, and charge accumulation was also monitored using TEM. The accumulation of charge led to the formation of frozen domains and shed light on ferroelectric degradation[185]. As another example, *in situ* electrical biasing experiments were conducted on an (La,Sr)MnO_3/$Hf_{0.5}Zr_{0.5}O_2$/(La,Sr)MnO_3 capacitor at the atomic scale. Direct observation confirmed the reversibility of oxygen vacancy migration at the oxygen-reactive electrode, and it was revealed that the vacancy migration is intertwined with ferroelectric switching[184]. When *in situ* bright field (BF)-STEM imaging was performed at a field of 300 kV/cm, lateral creeping of the domain wall in Pt/Pb(Zr,Ti)O_3/(La,Sr)MnO_3 was observed as an image contrast[186]. In addition, another example, as shown in Figure 14, includes direct observations at the atomic scale using Fe ion displacements of $BiFeO_3$ ferroelectric domain switching when an electric field was applied[187].

Atomic scale imaging methods, such as negative spherical aberration imaging (NCSI) and STEM, provide a detailed view of structures such as unit cell-wide domain at the atomic level[188]. These techniques allow for a precise analysis of even the nanosized domains such as flux-closure domains[189,190] and their domain walls[154]. Through the analysis of ionic displacement and distortion at the atomic level, we gain a deeper insight into the structures. Unlike TEM, which analyzes phase information, these methods provide imaging of precise atomic structures, making them suitable for analyzing unique features in thin films, such as the polar nanoregions[191,192] in relaxor ferroelectric properties or distinct domain forms such as polar vortexes[121,193,194]. They are adopted for unveiling hidden information. Electric polarization could be determined by ionic displacements in the images, and structural features such as tetragonality and relative tilt and rotation angles are simultaneously characterized at the unit cell level[195].

In general, HAADF-STEM and annular BF (ABF)-STEM images are the widely adopted imaging modes in STEM. HAADF-STEM is a robust imaging mode that displays the atomic number or Z-contrast of materials. The background of these images is dark, and thermally diffused scattered electron signals appear bright. It has been reported that the intensity of HAADF-STEM images is proportional to roughly 1.4~2 times the atomic number. However, it is challenging to observe light elements, such as oxygen, due to their low thermal diffuse scattering effect. ABF-STEM was introduced in a smaller annular form to address the difficulty HAADF-STEM has in detecting light elements. It has been revealed that ABF-STEM can image elements as light as hydrogen[196]. However, there are still challenges in imaging lighter elements due to issues such as aberration, defocus, tilt, and sample thickness.

eABF-STEM (enhanced ABF-STEM) is a newly developed technique designed for the sensitive visualization of light elements, offering improvements over the traditional ABF-STEM[197]. This method combines the advantages of both ABF-STEM and BF-STEM [Figure 15]. A BF-STEM image is generated from the scattered electron signal, where light elements appear bright and heavy elements appear dark. This is because heavy elements scatter farther from the center, while light elements scatter less. Although BF-STEM

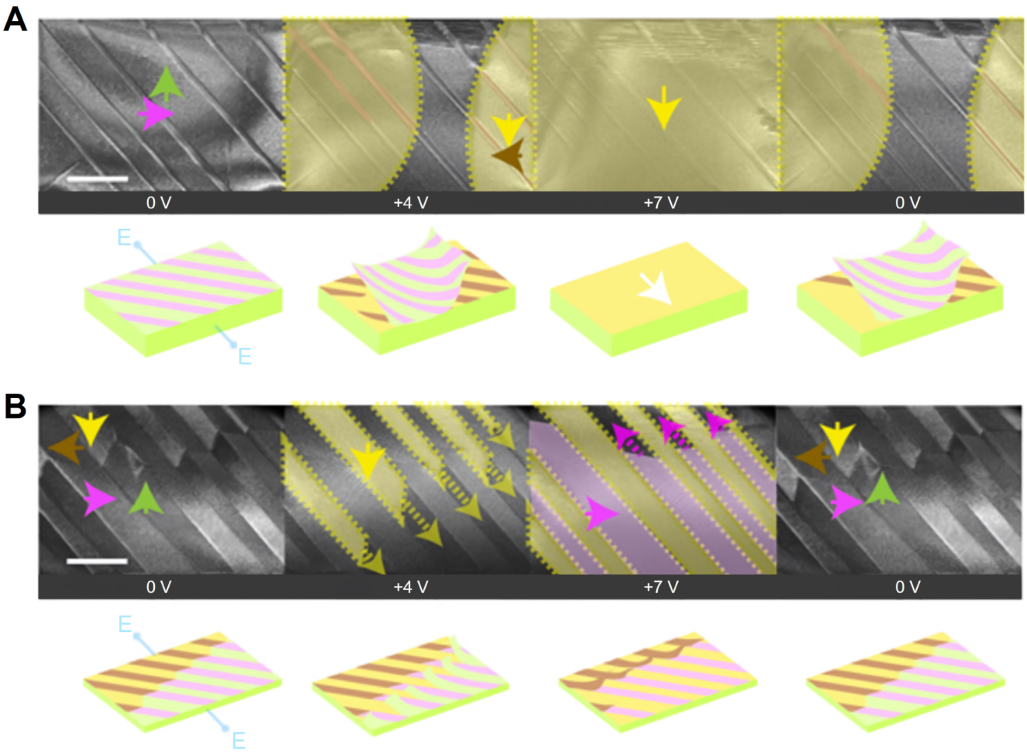

Figure 13. Thickness dependence of ferroelectric/ferroelastic domain switching under electric biasing. (A) Dark-field TEM images of thick TEM samples under the electric field. Yellow regions indicate the 180° domain switched regions. (B) Dark-field TEM images of thin TEM samples under the electric field. Pink regions indicate the 90° domain switched regions. Reproduced with permission[180]. Copyright 2020, The Authors, some rights reserved; exclusive licensee American Association for the Advancement of Science.

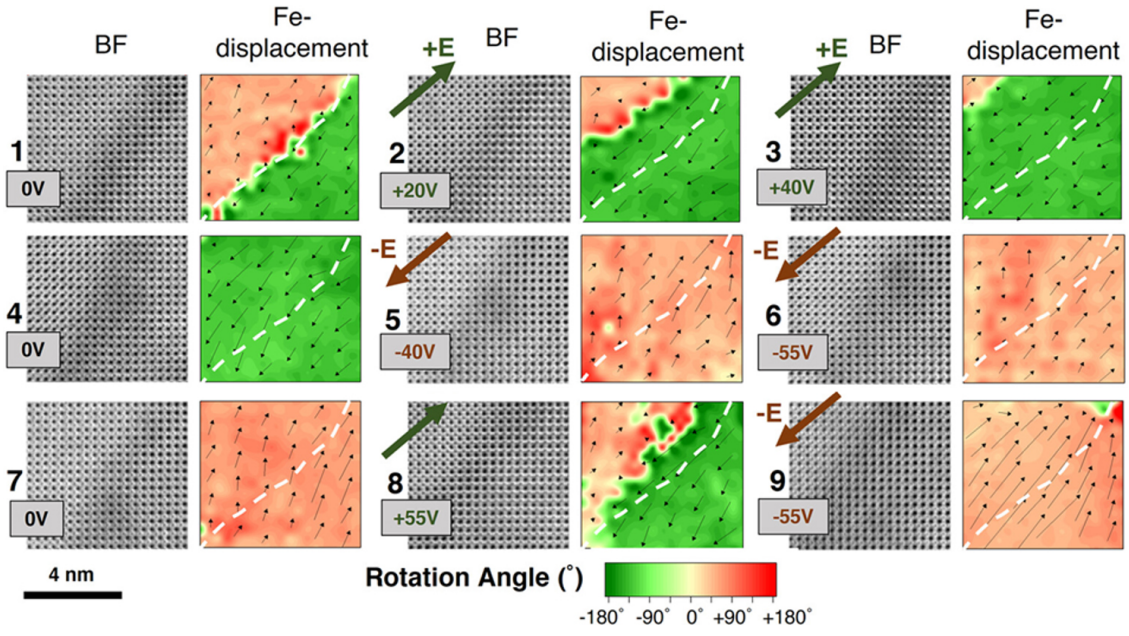

Figure 14. *In situ* BF-STEM image at the wall location together with Fe-displacement vectors superimposed on the color map of the Fe-displacement rotation angle. The sequence of applied voltages is numbered. Reproduced with permission[187]. Copyright 2022, The Authors, published by American Chemical Society.

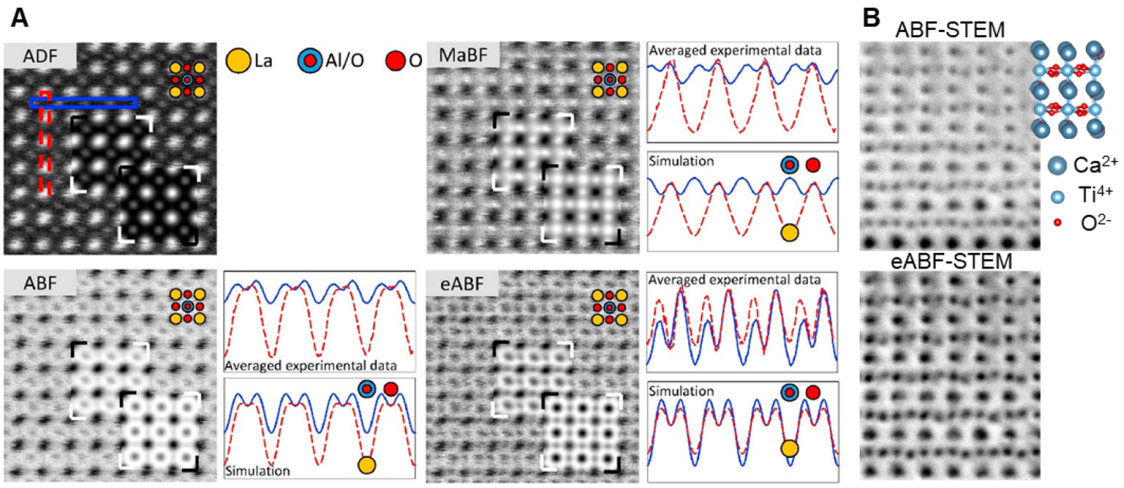

Figure 15. Four different STEM imaging modes. (A) STEM images of the $LaAlO_3$ with intensity profiles. Reproduced with permission[197]. Copyright 2013, Elsevier B.V. (B) Comparison between ABF- and eABF-STEM images of $CaTiO_3$ thin film.

is effective for detecting light elements, it can be challenging to accurately interpret atomic columns since intermediate weight elements are ambiguously displayed. In contrast, ABF-STEM displays dark signals at atomic columns against a bright background, making atomic columns intuitively recognizable. However, a drawback of ABF-STEM is the difficulty in observing light elements, as the incoherent effective source size diminishes the ABF-STEM signal. eABF-STEM is obtained by subtracting BF detector signals from ABF detector signals. While the overall signal intensity is reduced compared to ABF-STEM, the intensity difference between light and heavy elements increases, significantly enhancing the visibility of light elements. When eABF-STEM is utilized in ferroelectric materials, it is frequently used to demonstrate the relationship between the oxygen octahedra and ferroelectricity[198]. There has been a revelation using eABF-STEM about the gradual change in the oxygen octahedral tilt due to interface strain in the ferroelectric $Bi_{0.5}Na_{0.5}TiO_3$ thin film, and its association with the ferroelectric displacement of the Ti ion[199].

Moreover, advanced electron microscopy techniques, such as differential phase contrast (DPC) and 4D-STEM imaging using pixelated detectors, are being rapidly developed[200-203]. These techniques not only allow for the direct mapping of the internal electric field within materials but also enable imaging at higher resolutions[204]. DPC determines the phase shifts caused by interactions between the electron beam and the sample, enabling the detection of both electric and magnetic fields, as shown in Figure 16. Especially after it was revealed that atomic resolution could be achieved, there were expectations that the measurement of polarization would become possible[205]. Indeed, this capability was demonstrated in the material $BiFeO_3$, where the distribution of the electric field and the nature of polarization due to doping could be analyzed[200]. Research has been published illuminating the flexoelectric effect related electrical polarization mapping[201] and the non-Ising electric field distribution in ferroelectric domain walls[206] using DPC. In addition, a recent study highlighted the DPC in real-time to observe the atomic switching of ferroelectric wurtzite $Al_{0.94}B_{0.06}N$ induced by an electron beam[207].

The ferroelectric polarization can be observed over a large scale, but it can also manifest in very local structures. To analyze the subtle details visible in TEM images, software-based analysis techniques, such as deep learning, are being extensively researched alongside the development of TEM hardware[70,208]. Software-based techniques for atomic position analysis have been extensively studied to analyze factors such as polarization, relative displacement, distortion of the octahedra, and the lattice's tetragonality[209-212]

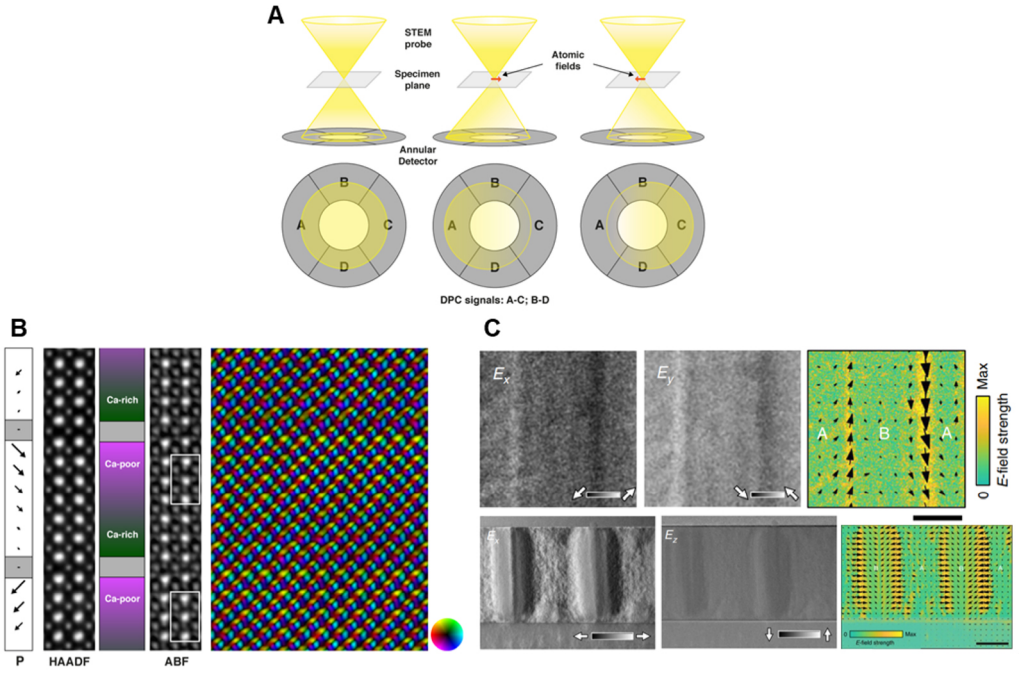

Figure 16. DPC-TEM measurements of electric fields. (A) Schematic representation of the basic principle of the DPC technique. (B) Vector plot of the atomic electric field in Ca-doped $BiFeO_3$. Reproduced with permission[200]. Copyright 2018, American Chemical Society. (C) Electric fields at the polar domain walls. Reproduced with permission[201]. Copyright 2020, The Authors, published by Springer Nature Limited.

[Figure 17]. The atomic positions can be determined using 2D quadratic fitting, Gaussian fitting, or the center of mass methods. Recently, techniques such as segmentation through k-means clustering based on unsupervised learning are also used to find atomic positions[208]. To extract precise peaks, the signal-to-noise ratio is improved using the Wiener filter in the frequency domain, especially for periodic images[213]. Advanced techniques such as nonlocal means denoising[214] and block matching and three-dimensional filtering (BM3D)[215,216] have also been employed. Currently, a significant portion of image analysis through peak detection has been automated, and the processing speed has greatly improved, alleviating many challenges in the structural analysis of ferroelectrics[208].

One of the strengths of deep learning-based analysis is that it allows for objective data analysis, eliminating human subjectivity; also, it is capable of processing vast amounts of data swiftly and efficiently. An example of applying deep learning to TEM research is its use in analyzing STEM images to understand the structure of the oxygen octahedra[70]. This research identified the $a^-b^+a^-$ and $a^-a^-a^-$ octahedral tilt structures in $CaTiO_3$ and linked them to ferroelectricity. Since STEM images are two-dimensional, they contain very subtle 3D structural information, which was meticulously analyzed. In addition, in a study involving polycrystalline $Hf_{0.5}Zr_{0.5}O_2$, deep learning was used on 4D-STEM data[217]. This revealed that it was possible to distinguish between the centrosymmetric monoclinic $P2_1/c$, tetragonal $P4_2/nmc$ phase, and the orthorhombic $Pca2_1$ phase with ferroelectric polarization in the TEM samples, disregarding factors such as thickness, tilt, and rotation. Similarly, an automated workflow using the ResNet 18 convolutional neural network technique was reported for classifying the monoclinic and orthorhombic phases in HZO to identify ferroelectric domains[218].

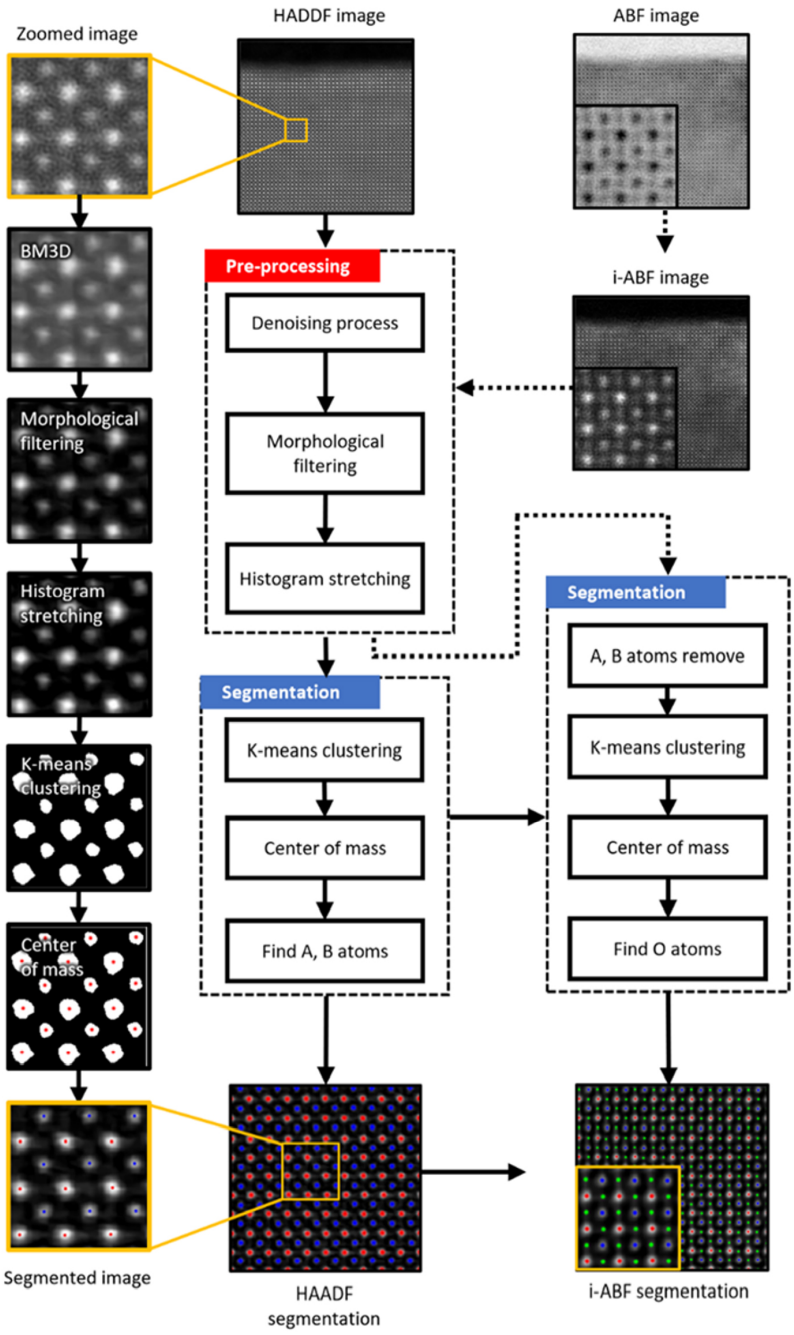

Figure 17. Example of machine learning-based STEM image analysis flowchart. Entire workflow of precise atomic peak analysis in parallelly acquired HAADF-STEM and ABF-STEM images of $SrTiO_3$. Preprocessing steps reduce noise and enhance the peak contrast, and segmentation steps achieve the coordinate information of atomic columns. Reproduced with permission[208]. Copyright 2022, The Authors, published by Springer Nature.

CONCLUSIONS

As the demand for advanced devices in the rapidly evolving information technology and artificial intelligence industries increases, pioneering a new class of miniaturized, high-functioning materials becomes a paramount research priority. With advancements now reaching the ultimate limits of materials, such as the unit cell or atomic levels, this review sheds light on various ferroelectric materials. These

materials are examined from both structural and domain perspectives, which are critical to ferroelectric research. We introduced the characteristics manifested in reduced structures. In particular, we highlighted the importance of the oxygen polyhedral structure as the cornerstone of oxide ferroelectric miniaturization. Moreover, we discuss the progressive advancements in sophisticated microscopy techniques vital for characterizing these miniaturized materials. In the future, it seems imperative to achieve breakthroughs that utilize atomic structures at the unit cell scale. Moving forward, there is a need to elucidate still-unknown challenges in operating unit cell-based devices stably and integrating them into real-world applications.

DECLARATIONS

Authors' contribution

Writing the original draft: Jang J
Reviewing and supervising: Choi SY

Availability of data and materials

Not applicable.

Financial support and sponsorship

This work was supported by Korea Basic Science Institute (National Research Facilities and Equipment Center) grant funded by the Ministry of Education (2020R1A6C101A202). This research was supported by the National R&D Program through the National Research Foundation of Korea (NRF) funded by the Ministry of Science and ICT (RS-2023-00258227).

Conflicts of interest

Both authors declared that there are no conflicts of interest.

Ethical approval and consent to participate

Not applicable.

Consent for publication

Not applicable.

REFERENCES

1. Scott JF. Applications of modern ferroelectrics. *Science* 2007;315:954-9. DOI PubMed
2. Guyonnet J, Gaponenko I, Gariglio S, Paruch P. Conduction at domain walls in insulating $Pb(Zr_{0.2}Ti_{0.8})O_3$ thin films. *Adv Mater* 2011;23:5377-82. DOI
3. Gao P, Nelson CT, Jokisaari JR, et al. Direct observations of retention failure in ferroelectric memories. *Adv Mater* 2012;24:1106-10. DOI
4. Valasek J. Piezo-electric and allied phenomena in rochelle salt. *Phys Rev* 1921;17:475-81. DOI
5. Shirane G, Takeda A. Phase transitions in solid solutions of $PbZrO_3$ and $PbTiO_3$ (I) small concentrations of $PbTiO_3$. *J Phys Soc Jpn* 1952;7:5-11. DOI
6. Nassau K, Levinstein HJ, Loiacono GM. Ferroelectric lithium niobate. 1. Growth, domain structure, dislocations and etching. *J Phys Chem Solids* 1966;27:983-8. DOI
7. Anderson JR. Ferroelectric materials as storage elements for digital computers and switching systems. *Trans AIEE Part I Comm Electron* 1953;71:395-401. DOI
8. Moll JL, Tarui Y. A new solid state memory resistor. *IEEE Trans Electron Devices* 1963;10:338. DOI
9. Dam B, Huijbregtse JM, Klaassen FC, et al. Origin of high critical currents in $YBa_2Cu_3O_{7-\delta}$ superconducting thin films. *Nature* 1999;399:439-42. DOI
10. Roas B, Schultz L, Endres G. Epitaxial growth of $YBa_2Cu_3O_{7-x}$ thin films by a laser evaporation process. *Appl Phys Lett*

1988;53:1557-9. DOI
11. de Araujo CAP, Cuchiaro JD, Mcmillan LD, Scott MC, Scott JF. Fatigue-free ferroelectric capacitors with platinum electrodes. *Nature* 1995;374:627-9. DOI
12. Fong DD, Stephenson GB, Streiffer SK, et al. Ferroelectricity in ultrathin perovskite films. *Science* 2004;304:1650-3. DOI
13. Wang J, Neaton JB, Zheng H, et al. Epitaxial $BiFeO_3$ multiferroic thin film heterostructures. *Science* 2003;299:1719-22. DOI
14. Lee D, Lu H, Gu Y, et al. Emergence of room-temperature ferroelectricity at reduced dimensions. *Science* 2015;349:1314-7. DOI
15. Cheng Y, Gao Z, Ye KH, et al. Reversible transition between the polar and antipolar phases and its implications for wake-up and fatigue in HfO_2-based ferroelectric thin film. *Nat Commun* 2022;13:645. DOI PubMed PMC
16. Böscke TS, Müller J, Bräuhaus D, Schröder U, Böttger U. Ferroelectricity in hafnium oxide thin films. *Appl Phys Lett* 2011;99:102903. DOI
17. Müller J, Böscke TS, Schröder U, et al. Ferroelectricity in simple binary ZrO_2 and HfO_2. *Nano Lett* 2012;12:4318-23. DOI
18. Müller J, Schröder U, Böscke TS, et al. Ferroelectricity in yttrium-doped hafnium oxide. *J Appl Phys* 2011;110:114113. DOI
19. Ji D, Cai S, Paudel TR, et al. Freestanding crystalline oxide perovskites down to the monolayer limit. *Nature* 2019;570:87-90. DOI
20. Guo Y, Goodge B, Zhang L, et al. Unit-cell-thick domain in free-standing quasi-two-dimensional ferroelectric material. *Phys Rev Mater* 2021;5:044403. DOI
21. Shirodkar SN, Waghmare UV. Emergence of ferroelectricity at a metal-semiconductor transition in a 1T monolayer of MoS_2. *Phys Rev Lett* 2014;112:157601. DOI
22. Chang K, Liu J, Lin H, et al. Discovery of robust in-plane ferroelectricity y in atomic-thick SnTe. *Science* 2016;353:274-8. DOI
23. Ding W, Zhu J, Wang Z, et al. Prediction of intrinsic two-dimensional ferroelectrics in In_2Se_3 and other III_2-VI_3 van der Waals materials. *Nat Commun* 2017;8:14956. DOI PubMed PMC
24. Liu F, You L, Seyler KL, et al. Room-temperature ferroelectricity in $CuInP_2S_6$ ultrathin flakes. *Nat Commun* 2016;7:12357. DOI PubMed PMC
25. Belianinov A, He Q, Dziaugys A, et al. $CuInP_2S_6$ room temperature layered ferroelectric. *Nano Lett* 2015;15:3808-14. DOI
26. Wang C, You L, Cobden D, Wang J. Towards two-dimensional van der Waals ferroelectrics. *Nat Mater* 2023;22:542-52. DOI
27. Merz WJ. The electric and optical behavior of $BaTiO_3$ single-domain crystals. *Phys Rev* 1949;76:1221-5. DOI
28. von Hippel A. Ferroelectricity, domain structure, and phase transitions of barium titanate. *Rev Mod Phys* 1950;22:221-37. DOI
29. Stern EA. Character of order-disorder and displacive components in barium titanate. *Phys Rev Lett* 2004;93:037601. DOI PubMed
30. Chaves A, Katiyar RS, Porto SPS. Coupled modes with A1 symmetry in tetragonal $BaTiO_3$. *Phys Rev B* 1974;10:3522-33. DOI
31. Comes R, Lambert M, Guinier A. The chain structure of $BaTiO_3$ and $KNbO_3$. *Solid State Commun* 1968;6:715-9. DOI
32. Buscaglia V, Buscaglia MT, Viviani M, et al. Raman and AFM piezoresponse study of dense $BaTiO_3$ nanocrystalline ceramics. *J Eur Ceram Soc* 2005;25:3059-62. DOI
33. Baskaran N, Ghule A, Bhongale C, Murugan R, Chang H. Phase transformation studies of ceramic $BaTiO_3$ using thermo-Raman and dielectric constant measurements. *J Appl Phys* 2002;91:10038-43. DOI
34. Slater JC. Theory of the transition in KH_2PO_4. *J Chem Phys* 1941;9:16-33. DOI
35. Sawada S, Nomura S, Fujii S, Yoshida I. Ferroelectricity in $NaNO_2$. *Phys Rev Lett* 1958;1:320-1. DOI
36. Neaton JB, Ederer C, Waghmare UV, Spaldin NA, Rabe KM. First-principles study of spontaneous polarization in multiferroic $BiFeO_3$. *Phys Rev B* 2005;71:014113. DOI
37. Lee HN, Nakhmanson SM, Chisholm MF, Christen HM, Rabe KM, Vanderbilt D. Suppressed dependence of polarization on epitaxial strain in highly polar ferroelectrics. *Phys Rev Lett* 2007;98:217602. DOI PubMed
38. Azuma M, Hojo H, Oka K, et al. Functional transition metal perovskite oxides with $6s^2$ lone pair activity stabilized by high-pressure synthesis. *Annu Rev Mater Res* 2021;51:329-49. DOI
39. Benedek NA, Fennie CJ. Why are there so few perovskite ferroelectrics? *J Phys Chem C* 2013;117:13339-49. DOI
40. Van Aken BB, Palstra TTM, Filippetti A, Spaldin NA. The origin of ferroelectricity in magnetoelectric $YMnO_3$. *Nat Mater* 2004;3:164-70. DOI PubMed
41. Benedek NA, Fennie CJ. Hybrid improper ferroelectricity: a mechanism for controllable polarization-magnetization coupling. *Phys Rev Lett* 2011;106:107204. DOI PubMed
42. Kimura T, Goto T, Shintani H, Ishizaka K, Arima T, Tokura Y. Magnetic control of ferroelectric polarization. *Nature* 2003;426:55-8. DOI PubMed
43. Qiao H, Wang C, Choi WS, Park MH, Kim Y. Ultra-thin ferroelectrics. *Mater Sci Eng R Rep* 2021;145:100622. DOI
44. Ascher E, Schmid H, Tar D. Dielectric properties of boracites and evidence for ferroelectricity. *Solid State Commun* 1964;2:45-9. DOI
45. Schmid H, Rieder H, Ascher E. Magnetic susceptibilities of some 3D transition metal boracites. *Solid State Commun* 1965;3:327-30. DOI
46. McQuaid RGP, Campbell MP, Whatmore RW, Kumar A, Gregg JM. Injection and controlled motion of conducting domain walls in improper ferroelectric Cu-Cl boracite. *Nat Commun* 2017;8:15105. DOI PubMed PMC
47. Dowty E, Clark JR. Atomic displacements in ferroelectric trigonal and orthorhombic boracite structures. *Solid State Commun* 1972;10:543-8. DOI
48. Zimmermann A, Bollmann W, Schmid H. Observations of ferroelectric domains in boracites. *Phys Stat Sol* 1970;3:707-20. DOI
49. Guy JGM, Cochard C, Aguado-Puente P, et al. Anomalous motion of charged domain walls and associated negative capacitance in

copper-chlorine boracite. *Adv Mater* 2021;33:e2008068. DOI

50. Bousquet E, Dawber M, Stucki N, et al. Improper ferroelectricity in perovskite oxide artificial superlattices. *Nature* 2008;452:732-6. DOI
51. Kumagai Y, Spaldin NA. Structural domain walls in polar hexagonal manganites. *Nat Commun* 2013;4:1540. DOI PubMed
52. Yoshida S, Fujita K, Akamatsu H, et al. Ferroelectric $Sr_3Zr_2O_7$: competition between hybrid improper ferroelectric and antiferroelectric mechanisms. *Adv Funct Mater* 2018;28:1801856. DOI
53. Benedek NA, Rondinelli JM, Djani H, Ghosez P, Lightfoot P. Understanding ferroelectricity in layered perovskites: new ideas and insights from theory and experiments. *Dalton Trans* 2015;44:10543-58. DOI PubMed
54. Roh CJ, Jung MC, Kim JR, et al. Polar metal phase induced by oxygen octahedral network relaxation in oxide thin films. *Small* 2020;16:e2003055. DOI
55. Jeong SG, Han G, Song S, et al. Propagation control of octahedral tilt in $SrRuO_3$ via artificial heterostructuring. *Adv Sci* 2020;7:2001643. DOI PubMed PMC
56. Geng WR, Guo XW, Zhu YL, et al. Oxygen octahedral coupling mediated ferroelectric-antiferroelectric phase transition based on domain wall engineering. *Acta Mater* 2020;198:145-52. DOI
57. Han H, Zhang Q, Li W, et al. Interfacial oxygen octahedral coupling-driven robust ferroelectricity in epitaxial $Na_{0.5}Bi_{0.5}TiO_3$ thin films. *Research* 2023;6:0191. DOI PubMed PMC
58. Sando D, Barthélémy A, Bibes M. $BiFeO_3$ epitaxial thin films and devices: past, present and future. *J Phys Condens Matter* 2014;26:473201. DOI PubMed
59. Jang BK, Lee JH, Chu K, et al. Electric-field-induced spin disorder-to-order transition near a multiferroic triple phase point. *Nat Phys* 2017;13:189-96. DOI
60. Chen D, Nelson CT, Zhu X, et al. A strain-driven antiferroelectric-to-ferroelectric phase transition in La-doped $BiFeO_3$ thin films on Si. *Nano Lett* 2017;17:5823-9. DOI
61. Chu K, Jang BK, Sung JH, et al. Enhancement of the anisotropic photocurrent in ferroelectric oxides by strain gradients. *Nat Nanotechnol* 2015;10:972-9. DOI
62. Glazer AM. The classification of tilted octahedra in perovskites. *Acta Cryst B* 1972;B28:3384-92. DOI
63. Han MJ, Wang YJ, Ma DS, et al. Coexistence of rhombohedral and orthorhombic phases in ultrathin $BiFeO_3$ films driven by interfacial oxygen octahedral coupling. *Acta Mater* 2018;145:220-6. DOI
64. Kim YM, Kumar A, Hatt A, et al. Interplay of octahedral tilts and polar order in $BiFeO_3$ films. *Adv Mater* 2013;25:2497-504. DOI
65. Yuan Y, Lu Y, Stone G, et al. Three-dimensional atomic scale electron density reconstruction of octahedral tilt epitaxy in functional perovskites. *Nat Commun* 2018;9:5220. DOI PubMed PMC
66. Yashima M, Ali R. Structural phase transition and octahedral tilting in the calcium titanate perovskite $CaTiO_3$. *Solid State Ion* 2009;180:120-6. DOI
67. Van Aert S, Turner S, Delville R, Schryvers D, Van Tendeloo G, Salje EKH. Direct observation of ferrielectricity at ferroelastic domain boundaries in $CaTiO_3$ by electron microscopy. *Adv Mater* 2012;24:523-7. DOI PubMed
68. Yokota H, Usami H, Haumont R, et al. Direct evidence of polar nature of ferroelastic twin boundaries in $CaTiO_3$ obtained by second harmonic generation microscope. *Phys Rev B* 2014;89:144109. DOI
69. Eklund CJ, Fennie CJ, Rabe KM. Strain-induced ferroelectricity in orthorhombic $CaTiO_3$ from first principles. *Phys Rev B* 2009;79:220101. DOI
70. Kim JR, Jang J, Go KJ, et al. Stabilizing hidden room-temperature ferroelectricity via a metastable atomic distortion pattern. *Nat Commun* 2020;11:4944. DOI PubMed PMC
71. Mitra C, Meyer T, Lee HN, Reboredo FA. Oxygen diffusion pathways in brownmillerite $SrCoO_{2.5}$: influence of structure and chemical potential. *J Chem Phys* 2014;141:084710. DOI PubMed
72. Fuller CA, Berrod Q, Frick B, et al. Brownmillerite-type Sr_2ScGaO_5 oxide ion conductor: local structure, phase transition, and dynamics. *Chem Mater* 2019;31:7395-404. DOI
73. Auckett JE, Studer AJ, Pellegrini E, et al. Combined experimental and computational study of oxide ion conduction dynamics in $Sr_2Fe_2O_5$ brownmillerite. *Chem Mater* 2013;25:3080-7. DOI
74. Macchesney JB, Sherwood RC, Potter JF. Electric and magnetic properties of the strontium ferrates. *J Chem Phys* 1965;43:1907-13. DOI
75. Khare A, Lee J, Park J, et al. Directing oxygen vacancy channels in $SrFeO_{2.5}$ epitaxial thin films. *ACS Appl Mater Interfaces* 2018;10:4831-7. DOI
76. Young J, Rondinelli JM. Crystal structure and electronic properties of bulk and thin film brownmillerite oxides. *Phys Rev B* 2015;92:174111. DOI
77. Lim J, Yu J. Role of oxygen vacancy in the spin-state change and magnetic ordering in $SrCoO_{3-\delta}$. *Phys Rev B* 2018;98:085106. DOI
78. Kang KT, Roh CJ, Lim J, et al. A room-temperature ferroelectric ferromagnet in a 1D tetrahedral chain network. *Adv Mater* 2019;31:e1808104. DOI
79. Tian H, Kuang XY, Mao AJ, et al. Novel type of ferroelectricity in brownmillerite structures: a first-principles study. *Phys Rev Mater* 2018;2:084402. DOI
80. Taniguchi H, Kuwabara A, Kim J, et al. Ferroelectricity driven by twisting of silicate tetrahedral chains. *Angew Chem Int Ed* 2013;52:8088-92. DOI

81. Seol D, Taniguchi H, Hwang JY, et al. Strong anisotropy of ferroelectricity in lead-free bismuth silicate. *Nanoscale* 2015;7:11561-5. DOI
82. Adams DM, Leonard S, Russell DR, Cernik RJ. X-ray diffraction study of Hafnia under high pressure using synchrotron radiation. *J Phys Chem Solids* 1991;52:1181-6. DOI
83. Sang X, Grimley ED, Schenk T, Schroeder U, Lebeau JM. On the structural origins of ferroelectricity in HfO_2 thin films. *Appl Phys Lett* 2015;106:162905. DOI
84. Smith SW, Kitahara AR, Rodriguez MA, Henry MD, Brumbach MT, Ihlefeld JF. Pyroelectric response in crystalline hafnium zirconium oxide ($Hf_{1-x}Zr_xO_2$) thin films. *Appl Phys Lett* 2017;110:072901. DOI
85. Lee HJ, Lee M, Lee K, et al. Scale-free ferroelectricity induced by flat phonon bands in HfO_2. *Science* 2020;369:1343-7. DOI
86. Mitsui T, Furuichi J. Domain structure of rochelle salt and KH_2PO_4. *Phys Rev* 1953;90:193-202. DOI
87. Guo EJ, Roth R, Herklotz A, Hesse D, Dörr K. Ferroelectric 180° domain wall motion controlled by biaxial strain. *Adv Mater* 2015;27:1615-8. DOI PubMed
88. Cruz MP, Chu YH, Zhang JX, et al. Strain control of domain-wall stability in epitaxial $BiFeO_3$ (110) films. *Phys Rev Lett* 2007;99:217601. DOI
89. Katayama K, Shimizu T, Sakata O, et al. Orientation control and domain structure analysis of {100}-oriented epitaxial ferroelectric orthorhombic HfO_2-based thin films. *J Appl Phys* 2016;119:134101. DOI
90. Gradauskaite E, Hunnestad KA, Meier QN, Meier D, Trassin M. Ferroelectric domain engineering using structural defect ordering. *Chem Mater* 2022;34:6468-75. DOI
91. Li L, Jokisaari JR, Zhang Y, et al. Control of domain structures in multiferroic thin films through defect engineering. *Adv Mater* 2018;30:e1802737. DOI
92. Baek SH, Jang HW, Folkman CM, et al. Ferroelastic switching for nanoscale non-volatile magnetoelectric devices. *Nat Mater* 2010;9:309-14. DOI
93. Nelson CT, Winchester B, Zhang Y, et al. Spontaneous vortex nanodomain arrays at ferroelectric heterointerfaces. *Nano Lett* 2011;11:828-34. DOI
94. Chouprik A, Spiridonov M, Zarubin S, et al. Wake-up in a $Hf_{0.5}Zr_{0.5}O_2$ film: a cycle-by-cycle emergence of the remnant polarization via the domain depinning and the vanishing of the anomalous polarization switching. *ACS Appl Electron Mater* 2019;1:275-87. DOI
95. Choudhury S, Li Y, Odagawa N, et al. The influence of 180° ferroelectric domain wall width on the threshold field for wall motion. *J Appl Phys* 2008;104:084107. DOI
96. Zhang Q, Tan G, Gu L, et al. Direct observation of multiferroic vortex domains in $YMnO_3$. *Sci Rep* 2013;3:2741. DOI PubMed PMC
97. Seidel J, Martin LW, He Q, et al. Conduction at domain walls in oxide multiferroics. *Nat Mater* 2009;8:229-34. DOI
98. Rojac T, Bencan A, Drazic G, et al. Domain-wall conduction in ferroelectric $BiFeO_3$ controlled by accumulation of charged defects. *Nat Mater* 2017;16:322-7. DOI
99. Aschauer U, Pfenninger R, Selbach SM, Grande T, Spaldin NA. Strain-controlled oxygen vacancy formation and ordering in $CaMnO_3$. *Phys Rev B* 2013;88:054111. DOI
100. Farokhipoor S, Noheda B. Conduction through 71° domain walls in $BiFeO_3$ thin films. *Phys Rev Lett* 2011;107:127601. DOI PubMed
101. Sluka T, Tagantsev AK, Bednyakov P, Setter N. Free-electron gas at charged domain walls in insulating $BaTiO_3$. *Nat Commun* 2013;4:1808. DOI PubMed PMC
102. Mundy JA, Schaab J, Kumagai Y, et al. Functional electronic inversion layers at ferroelectric domain walls. *Nat Mater* 2017;16:622-7. DOI
103. Crassous A, Sluka T, Tagantsev AK, Setter N. Polarization charge as a reconfigurable quasi-dopant in ferroelectric thin films. *Nat Nanotechnol* 2015;10:614-8. DOI PubMed
104. Oh YS, Luo X, Huang FT, Wang Y, Cheong SW. Experimental demonstration of hybrid improper ferroelectricity and the presence of abundant charged walls in $(Ca,Sr)_3Ti_2O_7$ crystals. *Nat Mater* 2015;14:407-13. DOI PubMed
105. Lee WM, Sung JH, Chu K, et al. Spatially resolved photodetection in leaky ferroelectric $BiFeO_3$. *Adv Mater* 2012;24:OP49-53. DOI
106. Sluka T, Tagantsev AK, Damjanovic D, Gureev M, Setter N. Enhanced electromechanical response of ferroelectrics due to charged domain walls. *Nat Commun* 2012;3:748. DOI PubMed PMC
107. McConville JPV, Lu H, Wang B, et al. Ferroelectric domain wall memristor. *Adv Funct Mater* 2020;30:2000109. DOI PubMed PMC
108. Liu Z, Wang H, Li M, et al. In-plane charged domain walls with memristive behaviour in a ferroelectric film. *Nature* 2023;613:656-61. DOI
109. Fiebig M, Lottermoser T, Fröhlich D, Goltsev AV, Pisarev RV. Observation of coupled magnetic and electric domains. *Nature* 2002;419:818-20. DOI PubMed
110. Choi T, Horibe Y, Yi HT, Choi YJ, Wu W, Cheong SW. Insulating interlocked ferroelectric and structural antiphase domain walls in multiferroic $YMnO_3$. *Nat Mater* 2010;9:253-8. DOI PubMed
111. Cheng S, Li J, Han MG, et al. Topologically allowed nonsixfold vortices in a sixfold multiferroic material: observation and classification. *Phys Rev Lett* 2017;118:145501. DOI
112. Du Y, Wang XL, Chen DP, et al. Domain wall conductivity in oxygen deficient multiferroic $YMnO_3$ single crystals. *Appl Phys Lett*

2011;99:252107. DOI
113. Matsumoto T, Ishikawa R, Tohei T, et al. Multivariate statistical characterization of charged and uncharged domain walls in multiferroic hexagonal $YMnO_3$ single crystal visualized by a spherical aberration-corrected STEM. *Nano Lett* 2013;13:4594-601. DOI
114. Småbråten DR, Meier QN, Skjærvø SH, Inzani K, Meier D, Selbach SM. Charged domain walls in improper ferroelectric hexagonal manganites and gallates. *Phys Rev Mater* 2018;2:114405. DOI
115. Xu X, Huang FT, Qi Y, et al. Kinetically stabilized ferroelectricity in bulk single-crystalline HfO_2:Y. *Nat Mater* 2021;20:826-32. DOI
116. Lee TY, Lee K, Lim HH, et al. Ferroelectric polarization-switching dynamics and wake-up effect in Si-doped HfO_2. *ACS Appl Mater Interfaces* 2019;11:3142-9. DOI
117. Grimley ED, Schenk T, Mikolajick T, Schroeder U, Lebeau JM. Atomic structure of domain and interphase boundaries in ferroelectric HfO_2. *Adv Mater Inter* 2018;5:1701258. DOI
118. Ding W, Zhang Y, Tao L, Yang Q, Zhou Y. The atomic-scale domain wall structure and motion in HfO_2-based ferroelectrics: a first-principle study. *Acta Mater* 2020;196:556-64. DOI
119. Chen S, Yuan S, Hou Z, et al. Recent progress on topological structures in ferroic thin films and heterostructures. *Adv Mater* 2021;33:e2000857. DOI
120. Tang YL, Zhu YL, Ma XL, et al. Ferroelectrics. Observation of a periodic array of flux-closure quadrants in strained ferroelectric $PbTiO_3$ films. *Science* 2015;348:547-51. DOI
121. Yadav AK, Nelson CT, Hsu SL, et al. Observation of polar vortices in oxide superlattices. *Nature* 2016;530:198-201. DOI
122. Das S, Tang YL, Hong Z, et al. Observation of room-temperature polar skyrmions. *Nature* 2019;568:368-72. DOI
123. Wang YJ, Feng YP, Zhu YL, et al. Polar meron lattice in strained oxide ferroelectrics. *Nat Mater* 2020;19:881-6. DOI
124. Luk'yanchuk I, Tikhonov Y, Razumnaya A, Vinokur VM. Hopfions emerge in ferroelectrics. *Nat Commun* 2020;11:2433. DOI PubMed PMC
125. Naumov II, Bellaiche L, Fu H. Unusual phase transitions in ferroelectric nanodisks and nanorods. *Nature* 2004;432:737-40. DOI PubMed
126. Fu H, Bellaiche L. Ferroelectricity in barium titanate quantum dots and wires. *Phys Rev Lett* 2003;91:257601. DOI PubMed
127. Choi KJ, Biegalski M, Li YL, et al. Enhancement of ferroelectricity in strained $BaTiO_3$ thin films. *Science* 2004;306:1005-9. DOI
128. Lee JH, Kim HJ, Ryoo E, et al. Thickness-driven morphotropic phase transition in metastable ferroelectric $CaTiO_3$ films. *Adv Elect Mater* 2022;8:2101398. DOI
129. Ahn CH, Rabe KM, Triscone JM. Ferroelectricity at the nanoscale: local polarization in oxide thin films and heterostructures. *Science* 2004;303:488-91. DOI PubMed
130. Stengel M, Spaldin NA. Origin of the dielectric dead layer in nanoscale capacitors. *Nature* 2006;443:679-82. DOI PubMed
131. Chang LW, Alexe M, Scott JF, Gregg JM. Settling the “dead layer” debate in nanoscale capacitors. *Adv Mater* 2009;21:4911-4. DOI PubMed
132. Saad MM, Baxter P, Bowman RM, Gregg JM, Morrison FD, Scott JF. Intrinsic dielectric response in ferroelectric nano-capacitors. *J Phys Condens Matter* 2004;16:L451-6. DOI
133. Stengel M, Vanderbilt D, Spaldin NA. Enhancement of ferroelectricity at metal-oxide interfaces. *Nat Mater* 2009;8:392-7. DOI PubMed
134. Junquera J, Ghosez P. Critical thickness for ferroelectricity in perovskite ultrathin films. *Nature* 2003;422:506-9. DOI PubMed
135. Gerra G, Tagantsev AK, Setter N, Parlinski K. Ionic polarizability of conductive metal oxides and critical thickness for ferroelectricity in $BaTiO_3$. *Phys Rev Lett* 2006;96:107603. DOI PubMed
136. Streiffer SK, Eastman JA, Fong DD, et al. Observation of nanoscale 180 degrees stripe domains in ferroelectric $PbTiO_3$ thin films. *Phys Rev Lett* 2002;89:067601. DOI
137. Gao P, Zhang Z, Li M, et al. Possible absence of critical thickness and size effect in ultrathin perovskite ferroelectric films. *Nat Commun* 2017;8:15549. DOI PubMed PMC
138. Zeches RJ, Rossell MD, Zhang JX, et al. A strain-driven morphotropic phase boundary in $BiFeO_3$. *Science* 2009;326:977-80. DOI
139. Li L, Cheng X, Blum T, et al. Observation of strong polarization enhancement in ferroelectric tunnel junctions. *Nano Lett* 2019;19:6812-8. DOI
140. Wang H, Liu ZR, Yoong HY, et al. Direct observation of room-temperature out-of-plane ferroelectricity and tunneling electroresistance at the two-dimensional limit. *Nat Commun* 2018;9:3319. DOI PubMed PMC
141. Sai N, Fennie CJ, Demkov AA. Absence of critical thickness in an ultrathin improper ferroelectric film. *Phys Rev Lett* 2009;102:107601. DOI
142. Sheng Z, Ogawa N, Ogimoto Y, Miyano K. Multiple stable states with in-plane anisotropy in ultrathin $YMnO_3$ films. *Adv Mater* 2010;22:5507-11. DOI PubMed
143. Yun Y, Buragohain P, Thind AS, et al. Spontaneous polarization in an ultrathin improper-ferroelectric/dielectric bilayer in a capacitor structure at cryogenic temperatures. *Phys Rev Appl* 2022;18:034071. DOI
144. Yang Q, Hu J, Fang YW, et al. Ferroelectricity in layered bismuth oxide down to 1 nanometer. *Science* 2023;379:1218-24. DOI
145. Zhang Z, Hsu SL, Stoica VA, et al. Epitaxial ferroelectric $Hf_{0.5}Zr_{0.5}O_2$ with metallic pyrochlore oxide electrodes. *Adv Mater* 2021;33:e2105655. DOI

146. Yun Y, Buragohain P, Li M, et al. Intrinsic ferroelectricity in Y-doped HfO_2 thin films. *Nat Mater* 2022;21:903-9. DOI
147. Cheema SS, Kwon D, Shanker N, et al. Enhanced ferroelectricity in ultrathin films grown directly on silicon. *Nature* 2020;580:478-82. DOI
148. Cheema SS, Shanker N, Hsu SL, et al. Emergent ferroelectricity in subnanometer binary oxide films on silicon. *Science* 2022;376:648-52. DOI
149. Kittel C. Theory of the structure of ferromagnetic domains in films and small particles. *Phys Rev* 1946;70:965-71. DOI
150. Prosandeev S, Lisenkov S, Bellaiche L. Kittel law in $BiFeO_3$ ultrathin films: a first-principles-based study. *Phys Rev Lett* 2010;105:147603. DOI
151. Catalan G, Seidel J, Ramesh R, Scott JF. Domain wall nanoelectronics. *Rev Mod Phys* 2012;84:119-56. DOI
152. Schilling A, Adams TB, Bowman RM, Gregg JM, Catalan G, Scott JF. Scaling of domain periodicity with thickness measured in $BaTiO_3$ single crystal lamellae and comparison with other ferroics. *Phys Rev B* 2006;74:024115. DOI
153. Feigl L, Yudin P, Stolichnov I, et al. Controlled stripes of ultrafine ferroelectric domains. *Nat Commun* 2014;5:4677. DOI
154. Wei XK, Jia CL, Sluka T, Wang BX, Ye ZG, Setter N. Néel-like domain walls in ferroelectric $Pb(Zr,Ti)O_3$ single crystals. *Nat Commun* 2016;7:12385. DOI PubMed PMC
155. De Luca G, Rossell MD, Schaab J, Viart N, Fiebig M, Trassin M. Domain wall architecture in tetragonal ferroelectric thin films. *Adv Mater* 2017;29:1605145. DOI PubMed
156. Cherifi-Hertel S, Bulou H, Hertel R, et al. Non-ising and chiral ferroelectric domain walls revealed by nonlinear optical microscopy. *Nat Commun* 2017;8:15768. DOI PubMed PMC
157. Han MG, Zhu Y, Wu L, et al. Ferroelectric switching dynamics of topological vortex domains in a hexagonal manganite. *Adv Mater* 2013;25:2415-21. DOI
158. Schaab J, Skjærvø SH, Krohns S, et al. Electrical half-wave rectification at ferroelectric domain walls. *Nat Nanotechnol* 2018;13:1028-34. DOI
159. Holtz ME, Shapovalov K, Mundy JA, et al. Topological defects in hexagonal manganites: inner structure and emergent electrostatics. *Nano Lett* 2017;17:5883-90. DOI
160. Han M, Wang C, Niu K, et al. Continuously tunable ferroelectric domain width down to the single-atomic limit in bismuth tellurite. *Nat Commun* 2022;13:5903. DOI PubMed PMC
161. Hirai K, Aso R, Ozaki Y, et al. Melting of oxygen vacancy order at oxide-heterostructure interface. *ACS Appl Mater Interfaces* 2017;9:30143-8. DOI
162. Young J, Moon EJ, Mukherjee D, et al. Polar oxides without inversion symmetry through vacancy and chemical order. *J Am Chem Soc* 2017;139:2833-41. DOI
163. Kim S, Hwang G, Song K, et al. Inverse size-dependence of piezoelectricity in single $BaTiO_3$ nanoparticles. *Nano Energy* 2019;58:78-84. DOI
164. Lu H, Bark CW, Esque de los Ojos D, et al. Mechanical writing of ferroelectric polarization. *Science* 2012;336:59-61. DOI
165. Lu H, Tan Y, Richarz L, et al. Electromechanics of domain walls in uniaxial ferroelectrics. *Adv Funct Mater* 2023;33:2213684. DOI
166. Buragohain P, Erickson A, Mimura T, Shimizu T, Funakubo H, Gruverman A. Effect of film microstructure on domain nucleation and intrinsic switching in ferroelectric $Y:HfO_2$ thin film capacitors. *Adv Funct Mater* 2022;32:2108876. DOI
167. Gruverman A, Alexe M, Meier D. Piezoresponse force microscopy and nanoferroic phenomena. *Nat Commun* 2019;10:1661. DOI PubMed PMC
168. Christman JA, Woolcott RR, Kingon AI, Nemanich RJ. Piezoelectric measurements with atomic force microscopy. *Appl Phys Lett* 1998;73:3851-3. DOI
169. Kalinin SV, Morozovska AN, Chen LQ, Rodriguez BJ. Local polarization dynamics in ferroelectric materials. *Rep Prog Phys* 2010;73:056502. DOI
170. Jesse S, Baddorf AP, Kalinin SV. Switching spectroscopy piezoresponse force microscopy of ferroelectric materials. *Appl Phys Lett* 2006;88:062908. DOI
171. Gruverman A, Wu D, Scott JF. Piezoresponse force microscopy studies of switching behavior of ferroelectric capacitors on a 100-ns time scale. *Phys Rev Lett* 2008;100:097601. DOI PubMed
172. Harnagea C, Alexe M, Hesse D, Pignolet A. Contact resonances in voltage-modulated force microscopy. *Appl Phys Lett* 2003;83:338-40. DOI
173. Rodriguez BJ, Callahan C, Kalinin SV, Proksch R. Dual-frequency resonance-tracking atomic force microscopy. *Nanotechnology* 2007;18:475504. DOI
174. Jesse S, Kalinin SV, Proksch R, Baddorf AP, Rodriguez BJ. The band excitation method in scanning probe microscopy for rapid mapping of energy dissipation on the nanoscale. *Nanotechnology* 2007;18:435503. DOI
175. Choi HJ, Jang J, Jung SY, et al. Thermal stress-assisted annealing to improve the crystalline quality of an epitaxial YSZ buffer layer on Si. *J Mater Chem C* 2022;10:10027-36. DOI
176. Zhang Y, Tan Y, Sando D, et al. Controlled nucleation and stabilization of ferroelectric domain wall patterns in epitaxial (110) bismuth ferrite heterostructures. *Adv Funct Mater* 2020;30:2003571. DOI
177. Gao P, Nelson CT, Jokisaari JR, et al. Revealing the role of defects in ferroelectric switching with atomic resolution. *Nat Commun* 2011;2:591. DOI
178. Han MG, Marshall MS, Wu L, et al. Interface-induced nonswitchable domains in ferroelectric thin films. *Nat Commun* 2014;5:4693.

DOI PubMed PMC

179. Lee JK, Shin GY, Song K, et al. Direct observation of asymmetric domain wall motion in a ferroelectric capacitor. *Acta Mater* 2013;61:6765-77. DOI
180. Chen Z, Li F, Huang Q, et al. Giant tuning of ferroelectricity in single crystals by thickness engineering. *Sci Adv* 2020;6:eabc7156. DOI PubMed PMC
181. Lee H, Okello OFN, Kim GY, Song K, Choi SY. TEM sample preparation using micro-manipulator for in-situ MEMS experiment. *Appl Microsc* 2021;51:8. DOI PubMed PMC
182. Vogel A, Sarott MF, Campanini M, Trassin M, Rossell MD. Monitoring electrical biasing of $Pb(Zr_{0.2}Ti_{0.8})O_3$ ferroelectric thin films in situ by DPC-STEM imaging. *Materials* 2021;14:4749. DOI PubMed PMC
183. Zintler A, Kunz U, Pivak Y, et al. FIB based fabrication of an operative Pt/HfO_2/TiN device for resistive switching inside a transmission electron microscope. *Ultramicroscopy* 2017;181:144-9. DOI
184. Nukala P, Ahmadi M, Wei Y, et al. Reversible oxygen migration and phase transitions in hafnia-based ferroelectric devices. *Science* 2021;372:630-5. DOI
185. Huang Q, Chen Z, Cabral MJ, et al. Direct observation of nanoscale dynamics of ferroelectric degradation. *Nat Commun* 2021;12:2095. DOI PubMed PMC
186. Cai S, Guo C, Niu B, et al. In situ observation of domain wall lateral creeping in a ferroelectric capacitor. *Adv Funct Mater* 2023;33:2304606. DOI
187. Condurache O, Dražić G, Rojac T, et al. Atomic-level response of the domain walls in bismuth ferrite in a subcoercive-field regime. *Nano Lett* 2023;23:750-6. DOI PubMed PMC
188. Du H, Groh C, Jia CL, et al. Multiple polarization orders in individual twinned colloidal nanocrystals of centrosymmetric HfO_2. *Matter* 2021;4:986-1000. DOI
189. Jia CL, Urban KW, Alexe M, Hesse D, Vrejoiu I. Direct observation of continuous electric dipole rotation in flux-closure domains in ferroelectric $Pb(Zr,Ti)O_3$. *Science* 2011;331:1420-3. DOI PubMed
190. Jia CL, Jin L, Wang D, et al. Nanodomains and nanometer-scale disorder in multiferroic bismuth ferrite single crystals. *Acta Mater* 2015;82:356-68. DOI
191. Hwang SY, Lee GJ, Qi Y, et al. Enhanced thermal stability by short-range ordered ferroelectricity in $K_{0.5}Na_{0.5}NbO_3$-based piezoelectric oxides. *Mater Horiz* 2023;10:2656-66. DOI
192. Kim GY, Chu K, Sung KD, et al. Disordered ferroelectricity in the $PbTiO_3$/$SrTiO_3$ superlattice thin film. *APL Mater* 2017;5:066104. DOI
193. Gong FH, Tang YL, Wang YJ, et al. Absence of critical thickness for polar skyrmions with breaking the Kittel's law. *Nat Commun* 2023;14:3376. DOI PubMed PMC
194. Sun Y, Abid AY, Tan C, et al. Subunit cell-level measurement of polarization in an individual polar vortex. *Sci Adv* 2019;5:eaav4355. DOI PubMed PMC
195. Kim HP, Lee GJ, Jeong HY, et al. Symmetry-bridging phase as the mechanism for the large strains in relaxor-$PbTiO_3$ single crystals. *J Eur Ceram Soc* 2019;39:3327-31. DOI
196. Yoon H, Choi M, Lim TW, et al. Reversible phase modulation and hydrogen storage in multivalent VO_2 epitaxial thin films. *Nat Mater* 2016;15:1113-9. DOI
197. Findlay SD, Kohno Y, Cardamone LA, Ikuhara Y, Shibata N. Enhanced light element imaging in atomic resolution scanning transmission electron microscopy. *Ultramicroscopy* 2014;136:31-41. DOI PubMed
198. Liu C, Xu J, Zheng T, et al. Decoding the atomic-scale structural origin of large strain performance in BNT-6BT based relaxor ferroelectrics. *J Phys Chem Lett* 2023;14:6234-40. DOI
199. Chen F, Qian H, Sun X, et al. Atomic-scale insight into the epitaxial growth mechanism and interfacial coupling of BNT film prepared by hydrothermal synthesis. *J Mater Sci Technol* 2023;164:198-204. DOI
200. Campanini M, Erni R, Yang CH, Ramesh R, Rossell MD. Periodic giant polarization gradients in doped $BiFeO_3$ thin films. *Nano Lett* 2018;18:717-24. DOI PubMed
201. Yun S, Song K, Chu K, et al. Flexopiezoelectricity at ferroelastic domain walls in WO_3 films. *Nat Commun* 2020;11:4898. DOI PubMed PMC
202. Gao W, Addiego C, Wang H, et al. Real-space charge-density imaging with sub-ångström resolution by four-dimensional electron microscopy. *Nature* 2019;575:480-4. DOI
203. Huyan H, Addiego C, Yan X, et al. Direct observation of polarization-induced two-dimensional electron/hole gases at ferroelectric-insulator interface. *NPJ Quantum Mater* 2021;6:88. DOI
204. Campanini M, Trassin M, Ederer C, Erni R, Rossell MD. Buried in-plane ferroelectric domains in Fe-doped single-crystalline aurivillius thin films. *ACS Appl Electron Mater* 2019;1:1019-28. DOI
205. Shibata N, Findlay SD, Kohno Y, Sawada H, Kondo Y, Ikuhara Y. Differential phase-contrast microscopy at atomic resolution. *Nat Phys* 2012;8:611-5. DOI
206. Weymann C, Cherifi-hertel S, Lichtensteiger C, et al. Non-Ising domain walls in c-phase ferroelectric lead titanate thin films. *Phys Rev B* 2022;106:L241404. DOI
207. Calderon S 5th, Hayden J, Baksa SM, et al. Atomic-scale polarization switching in wurtzite ferroelectrics. *Science* 2023;380:1034-8. DOI

208. Han J, Go KJ, Jang J, Yang S, Choi SY. Materials property mapping from atomic scale imaging via machine learning based sub-pixel processing. *NPJ Comput Mater* 2022;8:196. DOI
209. Galindo PL, Kret S, Sanchez AM, et al. The peak Pairs algorithm for strain mapping from HRTEM images. *Ultramicroscopy* 2007;107:1186-93. DOI
210. Nord M, Vullum PE, MacLaren I, Tybell T, Holmestad R. Atomap: a new software tool for the automated analysis of atomic resolution images using two-dimensional Gaussian fitting. *Adv Struct Chem Imaging* 2017;3:9. DOI PubMed PMC
211. Zhang Q, Zhang LY, Jin CH, Wang YM, Lin F. CalAtom: a software for quantitatively analysing atomic columns in a transmission electron microscope image. *Ultramicroscopy* 2019;202:114-20. DOI
212. Wang Y, Salzberger U, Sigle W, Eren Suyolcu Y, van Aken PA. Oxygen octahedra picker: a software tool to extract quantitative information from STEM images. *Ultramicroscopy* 2016;168:46-52. DOI
213. Marks LD. Wiener-filter enhancement of noisy HREM images. *Ultramicroscopy* 1996;62:43-52. DOI PubMed
214. Wei DY, Yin CC. An optimized locally adaptive non-local means denoising filter for cryo-electron microscopy data. *J Struct Biol* 2010;172:211-8. DOI
215. Mevenkamp N, Binev P, Dahmen W, Voyles PM, Yankovich AB, Berkels B. Poisson noise removal from high-resolution STEM images based on periodic block matching. *Adv Struct Chem Imag* 2015;1:3. DOI
216. Dabov K, Foi A, Katkovnik V, Egiazarian K. Image denoising by sparse 3-D transform-domain collaborative filtering. *IEEE Trans Image Process* 2007;16:2080-95. DOI PubMed
217. Kim YH, Yang SH, Jeong M, et al. Hybrid deep learning crystallographic mapping of polymorphic phases in polycrystalline $Hf_{0.5}Zr_{0.5}O_2$ thin films. *Small* 2022;18:e2107620. DOI
218. Cheng Z, Xie X, Yang Y, et al. Neural network approach for ferroelectric hafnium oxide phase identification at the atomistic scale. *Mater Today Electron* 2023;3:100027. DOI